RESEARCH MEMORANDUM

EXPERIMENTAL INVESTIGATION AT HIGH SUBSONIC SPEEDS OF THE EFFECTS OF LEADING-EDGE RADIUS ON THE AERODYNAMIC CHARACTERISTICS OF A SWEPTBACK-WING—FUSELAGE COMBINATION WITH LEADING-EDGE FLAPS AND CHORD-EXTENSIONS

By Kenneth P. Spreemann

Langley Aeronautical Laboratory
Langley Field, Va.

NATIONAL ADVISORY COMMITTEE
FOR AERONAUTICS

WASHINGTON

July 21, 1955
Declassified May 22, 1957

NATIONAL ADVISORY COMMITTEE FOR AERONAUTICS

RESEARCH MEMORANDUM

EXPERIMENTAL INVESTIGATION AT HIGH SUBSONIC SPEEDS OF THE EFFECTS OF LEADING-EDGE RADIUS ON THE AERODYNAMIC CHARACTERISTICS OF A SWEPTBACK-WING—FUSELAGE COMBINATION WITH LEADING-EDGE FLAPS AND CHORD-EXTENSIONS

By Kenneth P. Spreemann

SUMMARY

A limited investigation was made at high subsonic speeds to determine the effects of wing leading-edge radius on the aerodynamic characteristics of a sweptback-wing—fuselage combination with leading-edge flaps and chord-extensions. The basic wing had 45° sweepback, aspect ratio 4, taper ratio 0.3, and NACA 65A006 airfoil section. The leading-edge shapes considered consisted of a sharp leading edge, a normal airfoil leading edge, and a leading edge formed by using three times the normal radius and fairing the new nose contour smoothly into the normal airfoil. The investigation was made in the Langley high-speed 7- by 10-foot tunnel over a Mach number range of 0.80 to 0.92 and an angle-of-attack range of -2° to 24°. Lift, drag, and pitching-moment data were obtained for all configurations with leading-edge flap deflections of 0° and 6°.

Over the speed range investigated, the wings with sharp and blunt leading edges possessed less desirable lift characteristics in comparison with those of the normal leading-edge radius wing. The sharp and blunt leading-edge wings gave higher drag and lower lift-drag ratios in the high-lift and angle-of-attack range. With nose flap undeflected, the sharp leading-edge wing provided slightly less leading-edge suction than the normal and blunt leading-edge wings in the high-lift range. With a nose flap deflection of 6°, the blunt wing achieved about 10 to 15 percent more leading-edge suction than either the sharp or normal leading-edge wings in the low-lift range. The pitching-moment characteristics of the model with or without chord-extensions were only slightly affected by the changes in leading-edge radius.

INTRODUCTION

Previous investigations of thin sweptback-wing models at high subsonic speeds have shown that the pitching-moment characteristics and lift-drag ratios could be substantially improved with combinations of leading-edge chord-extensions and flaps (refs. 1 and 2, for example). These improvements due to leading-edge chord-extensions and flaps probably arise from their effects on the leading-edge vortex pattern.

It has been shown in reference 3 that, at low speeds, leading-edge radius obtained by changing the airfoil maximum thickness ratio is another parameter that has a pronounced effect on the leading-edge vortex pattern. A practical application of this principle would be to change the leading-edge radius so as to affect only a small portion of the wing, thus precluding a change in the basic structure of an airplane wing. It was therefore deemed desirable to conduct a limited investigation at high subsonic speeds to determine the effects of leading-edge radius without changes in maximum thickness ratio on the pitching-moment characteristics and lift-drag ratios. The present investigation provides direct comparisons with published results of the same model with a normal leading-edge radius (ref. 1).

COEFFICIENTS AND SYMBOLS

All coefficients presented herein are based on the wing area without chord-extensions. The coefficients and symbols used in this paper are defined as follows:

C_L lift coefficient, $\frac{\text{Lift}}{qS}$

C_D drag coefficient, $\frac{\text{Drag}}{qS}$

C_m pitching-moment coefficient referred to $0.25\bar{c}$, $\frac{\text{Pitching moment}}{qS\bar{c}}$

C_{D_b} base-pressure drag coefficient

C_{m_o} pitching-moment coefficient at zero-lift coefficient

ΔC_D drag coefficient due to lift, $\left(C_D - C_{D_{(C_{L=0})}} \text{ at } \delta_n = 0^\circ\right)$

C_{D_i} theoretical induced drag coefficient $\left(1.0025 \frac{C_L^2}{\pi(AR)}\right.$, calculated by method of ref. 4$\left.\right)$

D_F equivalent leading-edge suction factor, $100\left(\frac{\frac{C_{L\alpha}}{57.3} - \Delta C_D}{\frac{C_{L\alpha}}{57.3} - C_{D_i}}\right)$

AR aspect ratio, b^2/S

q dynamic pressure, $\frac{1}{2}\rho V^2$, lb/sq ft

S wing area, sq ft (2.25 on model)

S_b area of base of model, sq ft (0.059 on model)

$\bar{c}$ mean aerodynamic chord of wing, $\frac{2}{S}\int_0^{b/2} c^2\,dy$, ft

c local wing chord, parallel to plane of symmetry, ft

b wing span, ft

ρ air density, slugs/cu ft

V free-stream velocity, ft/sec

p_o free-stream static pressure, lb/sq ft

p_b static pressure at base of model, lb/sq ft

M Mach number

R Reynolds number of wing based on $\bar{c}$

α angle of attack of fuselage center line, deg

δ_n leading-edge flap deflection angle parallel to free stream, deg (see fig. 1)

Flap designations:

A	leading-edge flap that extends from 0.139 $\frac{b}{2}$ to 0.65 $\frac{b}{2}$
B	leading-edge flap that extends from 0.65 $\frac{b}{2}$ to 1.00 $\frac{b}{2}$

MODELS AND APPARATUS

A drawing of the wing-fuselage combinations showing details of the leading-edge radii, chord-extension, and flaps employed is presented in figure 1. A photograph of the model equipped with 6° full-span leading-edge flap and chord-extension, mounted on the sting in the Langley high-speed 7- by 10-foot tunnel, is shown in figure 2. The wing employed in this investigation had 45° sweepback of the quarter-chord line, aspect ratio 4, taper ratio 0.3, and NACA 65A006 airfoil section parallel to the plane of symmetry. The changes in leading-edge radius were made by altering the airfoil section forward of the 20-percent-chord line for the sharp leading edge and forward of the 5-percent-chord line for the blunt leading edge as shown in figure 1. Ordinates of the fuselage are given in table I.

The leading-edge flap was established by cutting the wing along the 20-percent-chord line, and flap angles were obtained with preset steel inserts. After setting a desired flap angle, the groove in the wing was filled and finished flush to the wing surface. The junctures between flaps were sealed for all tests. Estimated static load measurements indicated that angular distortion of the flap under load was negligible.

The leading-edge chord-extension was made by moving the leading 20 percent of the wing forward $0.10\bar{c}$ over the outboard 0.35 $\frac{b}{2}$. The $0.10\bar{c}$ gap was faired from the rear of the nose portion to the original 20-percent-chord line.

The model was tested on the sting-type support system shown in figure 2. With this system the model was remotely operated through an angle-of-attack range from about -2° to 24°. A strain-gage balance mounted inside the fuselage was used to measure the forces and moments of the wing-fuselage combination.

TESTS AND CORRECTIONS

The investigation was made in the Langley high-speed 7- by 10-foot tunnel. Lift, drag, and pitching moment were measured through a Mach number range of 0.80 to 0.92 and an angle-of-attack range of about -2° to 24° for each configuration listed in table II. The size of the model caused the tunnel to choke at a corrected Mach number of about 0.95 for the zero-lift condition. Partial choking conditions may have occurred in the high angle-of-attack range at a Mach number of the order of 0.93.

Blockage corrections were determined by the method of reference 5 and were applied to the Mach numbers and dynamic pressures. Jet-boundary corrections, applied to the angle of attack and drag, were calculated by the method of reference 6. The angles of attack have been corrected for deflection of the sting-support system under load. The jet-boundary corrections to pitching moment were considered negligible and were not applied to the data. No corrections have been applied to the data for buoyancy due to longitudinal pressure gradients. Qualitative measurements of the pressure gradients have indicated that the drag coefficients may be too low by about 0.0017. No tare corrections have been applied to the data, since previous experience (ref. 7, for example) indicates that for a tailless sting-mounted model, similar to the model investigated herein, the tare corrections to lift and pitch are negligible.

The drag data have been adjusted to correspond to a pressure at the base of the fuselage equal to free-stream static pressure. For this adjustment, the base pressure was determined by measuring the pressure inside the fuselage at a point about 9 inches forward of the base. The drag increment (base-pressure drag coefficient C_{D_b}) was calculated from the measured pressure data by the relation $C_{D_b} = \frac{p_b - p_o}{q} \frac{S_b}{S}$. Values of C_{D_b} for average test conditions are presented in figure 3. The adjusted model drag data were obtained by adding the base-pressure drag coefficient to the drag coefficient determined from the strain-gage measurements.

The mean Reynolds number of this investigation varied from 3.08×10^6 to 3.15×10^6 at corresponding Mach numbers from 0.80 to 0.93.

RESULTS AND DISCUSSION

The data are presented in figures 4 to 13; a detailed listing of the data is given in table II. The data for the normal leading-edge

radius wing were taken directly from reference 1 and although there is no direct comparison above $M = 0.90$ it is believed that the data at $M = 0.93$ for the normal leading-edge radius wing will give a reasonably good basis for qualitative comparison with data of this investigation at $M = 0.92$.

Lift Characteristics

In the normally linear lift range, the sharp leading-edge lift-curve slopes were negligibly affected by leading-edge flaps up to $\delta_n = 6^\circ$, but at 10° and 15° there were noticeable increases in the lift-curve slopes (fig. 4(a)). Above about 8° angle of attack, generally C_L increased with δ_n except for $\delta_n = 15^\circ$ above $M = 0.90$.

The lift-curve slopes were not greatly affected by leading-edge radius at $\delta_n = 0^\circ$ (fig. 5(a)); however, at $\delta_n = 6^\circ$, the sharp and blunt leading-edge wings gave lower lift-curve slopes than the normal leading-edge radius wing. The sharp and blunt leading-edge wings also usually gave appreciably lower lift coefficients than the normal leading edge above about 6° to 8° angle of attack (fig. 5(a)).

Addition of the chord-extensions to the sharp leading-edge wing increased the lift-curve slopes (fig. 6(a)). Throughout the Mach number range investigated, the lift coefficients above 8° angle of attack were always increased with the addition of the chord-extensions regardless of the leading-edge radius. As previously noted, the sharp and blunt leading-edge wings gave the lowest lift coefficients above 6° or 8° angle of attack which also was true of the sharp leading-edge wing with chord-extensions added.

Drag Characteristics

The minimum drag coefficient of the sharp leading-edge wing was progressively increased with flap deflection (fig. 4(b)). Throughout the Mach number range investigated, the sharp and blunt leading-edge wings have higher drag above $C_L = 0.4$ than the normal leading-edge wing with the largest increases being evident at $\delta_n = 6^\circ$ (fig. 5(b)). The addition of chord-extensions to the model resulted in reductions of C_D above about $C_L = 0.3$ (fig. 6(b)). As was noted without chord-extensions, the sharp leading-edge wing with chord-extensions also gave higher drag than the normal leading-edge wing above $C_L = 0.4$.

It was observed in reference 1 that the leading-edge flap deflections of 3° and 6° gave the best overall lift-drag ratios for that

configuration (normal leading-edge wing), and in this investigation with the sharp leading edge the best overall lift-drag ratios were also obtained with 3° and 6° flaps. (See fig. 7.)

The lift-drag ratios at $\delta_n = 0°$ presented in figures 8 and 11 show that the blunt leading-edge wings gave lower $(L/D)_{max}$ values than the sharp and normal leading-edge wings; whereas for $\delta_n = 6°$ (figs. 9 and 12) the normal leading-edge wing gave the lowest $(L/D)_{max}$ values.

The parameter D_F (figs. 11 and 12) represents the percent of equivalent full leading-edge suction realized. It should be noted that at the higher lift coefficients the percent of equivalent leading-edge suction indicated by D_F probably is lower than the percent suction actually realized, inasmuch as the drag due to lift may be increased by trailing-edge separation as well as by losses in leading-edge suction. For $\delta_n = 0°$ at low lift coefficients (0.30 and lower), the drag due to lift ΔC_D was apparently little affected by leading-edge radius but, for $\delta_n = 6°$, ΔC_D was slightly lower with the blunt leading-edge wing. (See figs. 11 and 12.) The lower value of ΔC_D at $\delta_n = 6°$ in the low-lift range represents an achievement of about 10 to 15 percent greater leading-edge suction D_F than that obtained with the sharp or normal leading-edge wings. At higher lift coefficients, for example $C_L = 0.60$, the sharp leading-edge wing had higher drag due to lift below $M = 0.90$ than either the normal or blunt leading-edge wings for both flap conditions ($\delta_n = 0°$ and 6°). The higher value of ΔC_D for the sharp leading-edge wing resulted in slightly less leading-edge suction than that realized with the normal and blunt leading-edge wings. (See figs. 11 and 12.) In general, changes in leading-edge radius resulted in no large effects on the drag characteristics in the Mach number range investigated.

Pitching-Moment Characteristics

The unstable pitching-moment variation, usually referred to as pitch-up, was progressively delayed to higher lift coefficients and angles of attack by increases in nose flap deflection, except for $\delta_n = 15°$ above a Mach number of 0.90 (figs. 4(c) and 4(d)). Because at 15° flap deflection a rather abrupt juncture occurs at the flap hinge line, there probably exists a region for the start of separated flow.

The pitching-moment data of figures 5 and 6 indicate that in the Mach number range of this investigation leading-edge radius had little effect on the point of pitch-up with or without chord-extensions.

The summary of pitching moment for zero lift C_{m_o} given in figure 13 indicates that C_{m_o} was shifted negatively about 0.002 per degree of flap deflection. Changes in leading-edge radius had little overall effect on the pitching-moment characteristics of the model.

CONCLUSIONS

A limited investigation at high subsonic speed of the effects of leading-edge radius on the aerodynamic characteristics in pitch of a wing-fuselage configuration with a 45° sweptback wing of aspect ratio 4 and an NACA 65A006 airfoil section (with and without leading-edge flaps and chord-extensions) indicated the following conclusions:

1. The sharp and blunt leading-edge wings had less desirable lift characteristics compared with those of the normal leading-edge radius wing. However for the sharp and normal leading edge, the lift generally increased with increasing flap deflection above about 8° angle of attack.

2. The sharp and blunt leading-edge wings gave higher drag and lower lift-drag ratios than the normal leading-edge wing in the high-lift and angle-of-attack range.

3. With no leading-edge flap deflection, the sharp leading-edge wing provided slightly less leading-edge suction than the normal and blunt leading-edge wings in the high-lift range. With a flap deflection of 6°, the blunt wing achieved about 10 to 15 percent more leading-edge suction than either the sharp or normal leading-edge wings in the low-lift range.

4. The pitching-moment characteristics of the model with or without chord-extensions were only slightly affected by the changes in leading-edge radius.

Langley Aeronautical Laboratory,
National Advisory Committee for Aeronautics,
Langley Field, Va., May 6, 1955.

REFERENCES

1. Spreemann, Kenneth P., and Alford, William J., Jr.: Investigation of the Effects of Leading-Edge Chord-Extensions and Fences in Combination With Leading-Edge Flaps on the Aerodynamic Characteristics at Mach Numbers From 0.40 to 0.93 of a 45° Sweptback Wing of Aspect Ratio 4. NACA RM L53A09a, 1953.

2. Spreemann, Kenneth P., and Alford, William J., Jr.: Investigation of the Effects of Leading-Edge Flaps on the Aerodynamic Characteristics in Pitch at Mach Numbers From 0.40 to 0.93 of a Wing-Fuselage Configuration With a 45° Sweptback Wing of Aspect Ratio 4. NACA RM L53G13, 1953.

3. Furlong, G. Chester, and McHugh, James G.: A Summary and Analysis of the Low-Speed Longitudinal Characteristics of Swept Wings at High Reynolds Number. NACA RM L52D16, 1952.

4. DeYoung, John, and Harper, Charles W.: Theoretical Symmetric Span Loadings at Subsonic Speeds for Wings Having Arbitrary Plan Form. NACA Rep. 921, 1948.

5. Herriot, John G.: Blockage Corrections for Three-Dimensional-Flow Closed-Throat Wind Tunnels, With Consideration of the Effect of Compressibility. NACA Rep. 995, 1950. (Supersedes NACA RM A7B28.)

6. Gillis, Clarence L., Polhamus, Edward C., and Gray, Joseph L., Jr.: Charts for Determining Jet-Boundary Corrections for Complete Models in 7- by 10-Foot Closed Rectangular Wind Tunnels. NACA WR L-123, 1945. (Formerly NACA ARR L5G31.)

7. Osborne, Robert S.: High-Speed Wind-Tunnel Investigation of the Longitudinal Stability and Control Characteristics of a 1/16-Scale Model of the D-558-2 Research Airplane at High Subsonic Mach Numbers and at a Mach Number of 1.2. NACA RM L9C04, 1949.

TABLE I.- FUSELAGE ORDINATES

[Basic fineness ratio, 12; actual fineness ratio 9.8 achieved by cutting off rear portion of body]

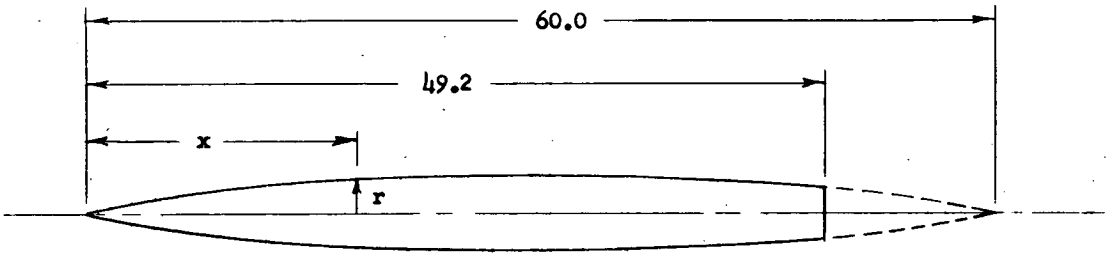

Ordinate, in.	
x	r
0	0
.30	.139
.45	.179
.75	.257
1.50	.433
3.00	.723
4.50	.968
6.00	1.183
9.00	1.556
12.00	1.854
15.00	2.079
18.00	2.245
21.00	2.360
24.00	2.438
27.00	2.486
30.00	2.500
33.00	2.478
36.00	2.414
39.00	2.305
42.00	2.137
49.20	1.650
L.E. radius = 0.030 in.	

TABLE II.- INDEX OF FIGURES PRESENTING DATA

Figure	δ_n, deg	Leading edge			Chord-extension	Data presented
		Sharp	Normal	Blunt		
4	0, 3, 6, 10, and 15	AB			None	Basic longitudinal
5	0 and 6	AB	AB	AB	None	Basic longitudinal
6	6	AB			None	Basic longitudinal
		AB	AB		0.65 $\frac{b}{2}$ to 1.00 $\frac{b}{2}$	
		A	B			
7	0, 3, 6, 10, and 15	AB			None	L/D
8	0	AB	AB	AB	None	L/D
9	6	AB	AB	AB	None	L/D
10	6	AB			None	L/D
		AB	AB		0.65 $\frac{b}{2}$ to 1.00 $\frac{b}{2}$	
		A	B			
11	0	AB	AB	AB	None	Summary of drag characteristics
12	6	AB	AB	AB	None	Summary of drag characteristics
13	0 to 15	AB	AB	AB	None	C_{m_o}

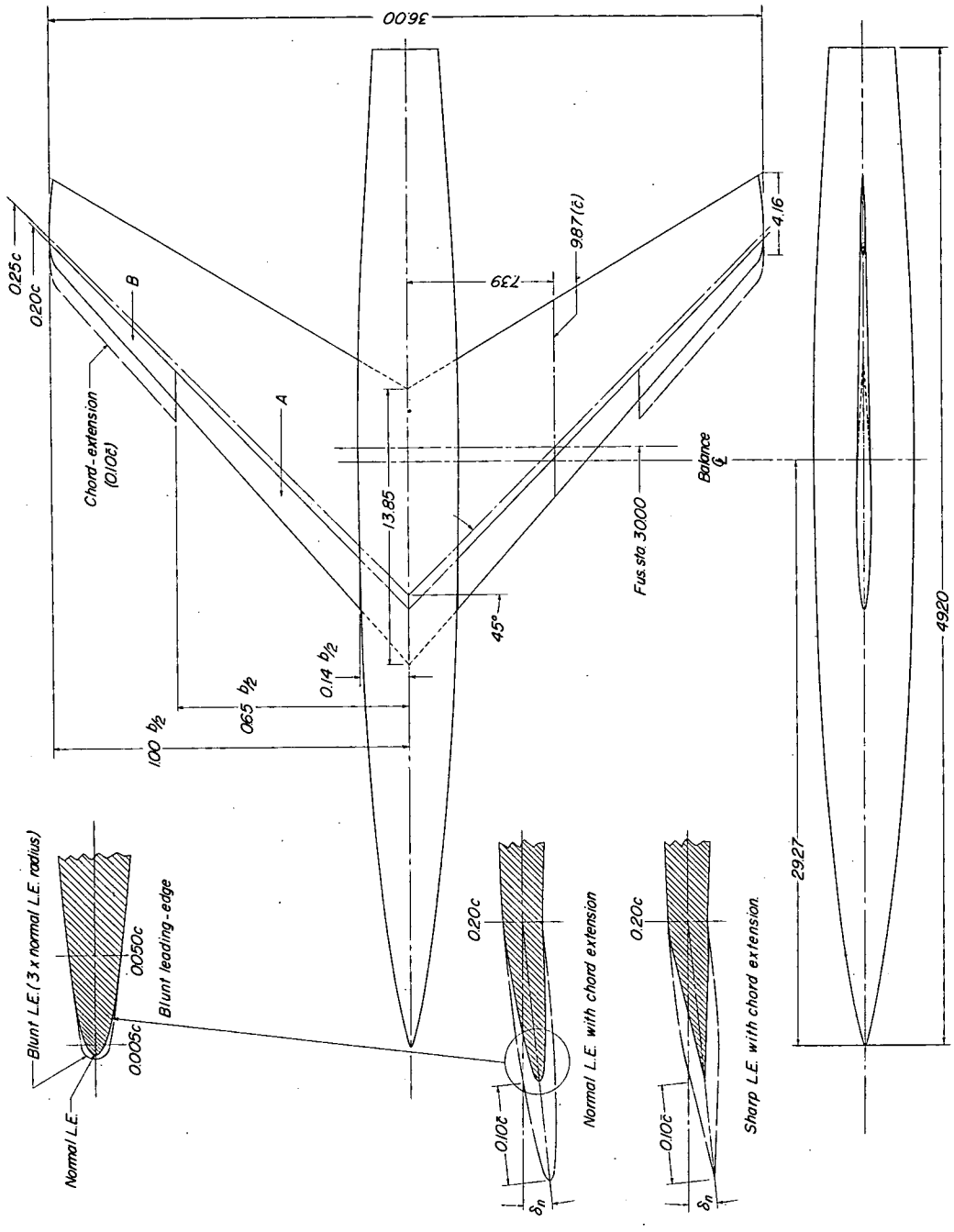

Figure 1.- Test model showing details of various wing leading-edge modifications employed.

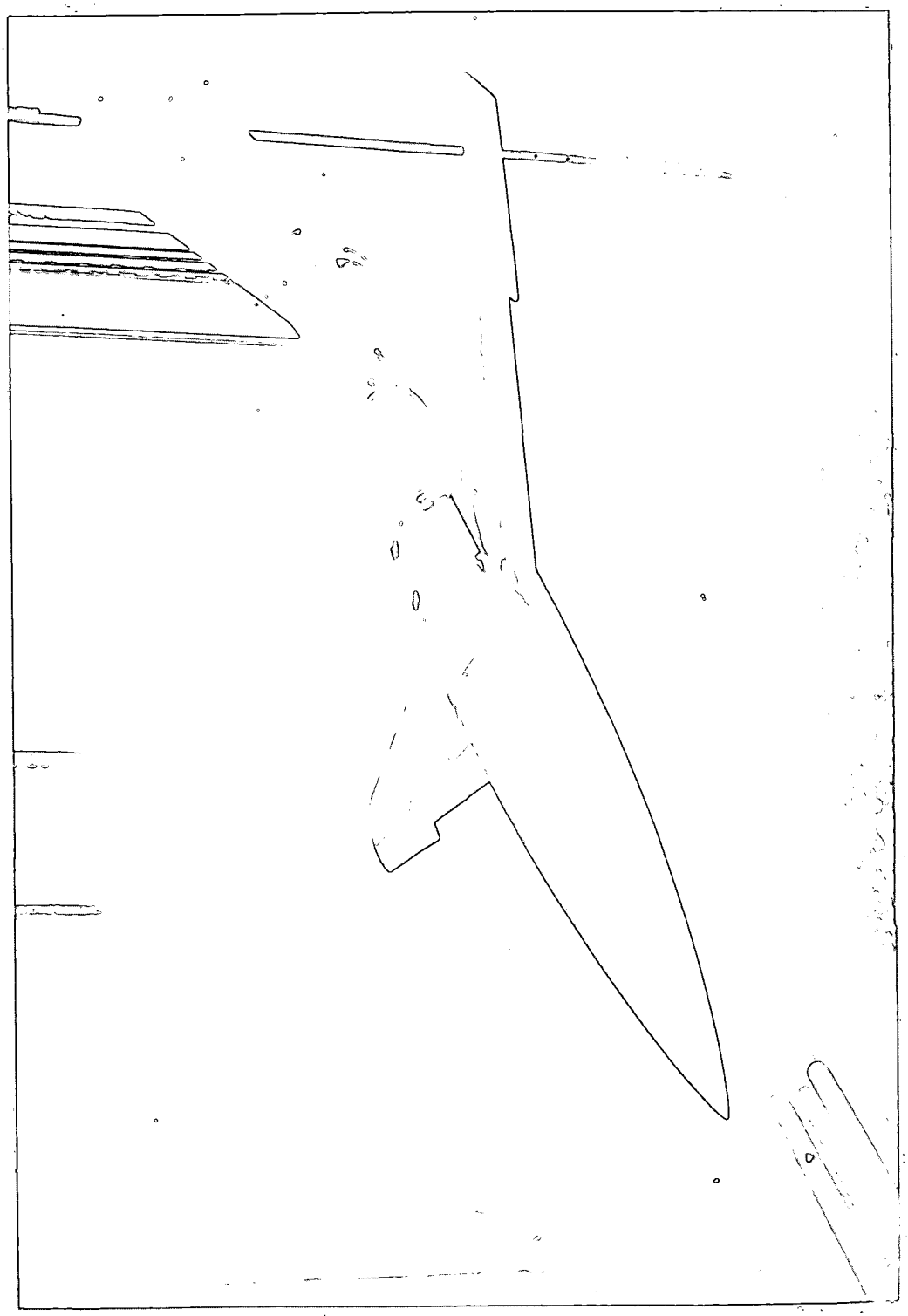

L-74562

Figure 2.- View of model mounted in Langley high-speed 7- by 10-foot tunnel showing 60° full-span flap with chord-extension from 0.65b/2 to tip.

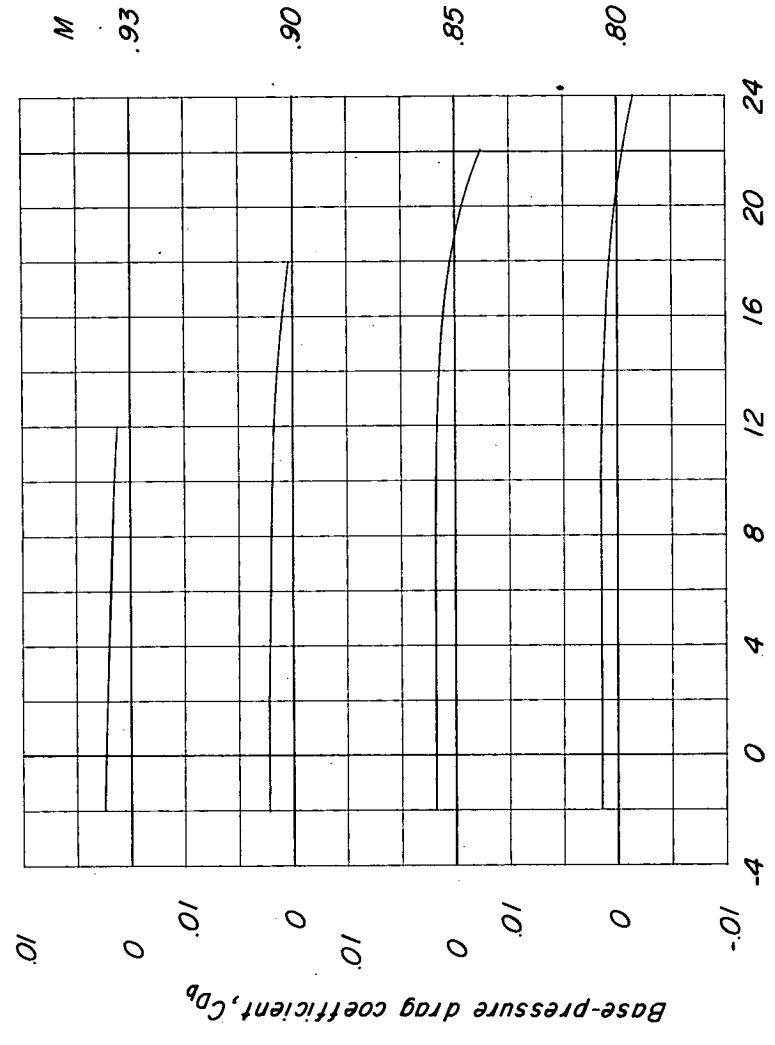

Figure 3.- Variation of base-pressure drag coefficient with angle of attack and test Mach number.

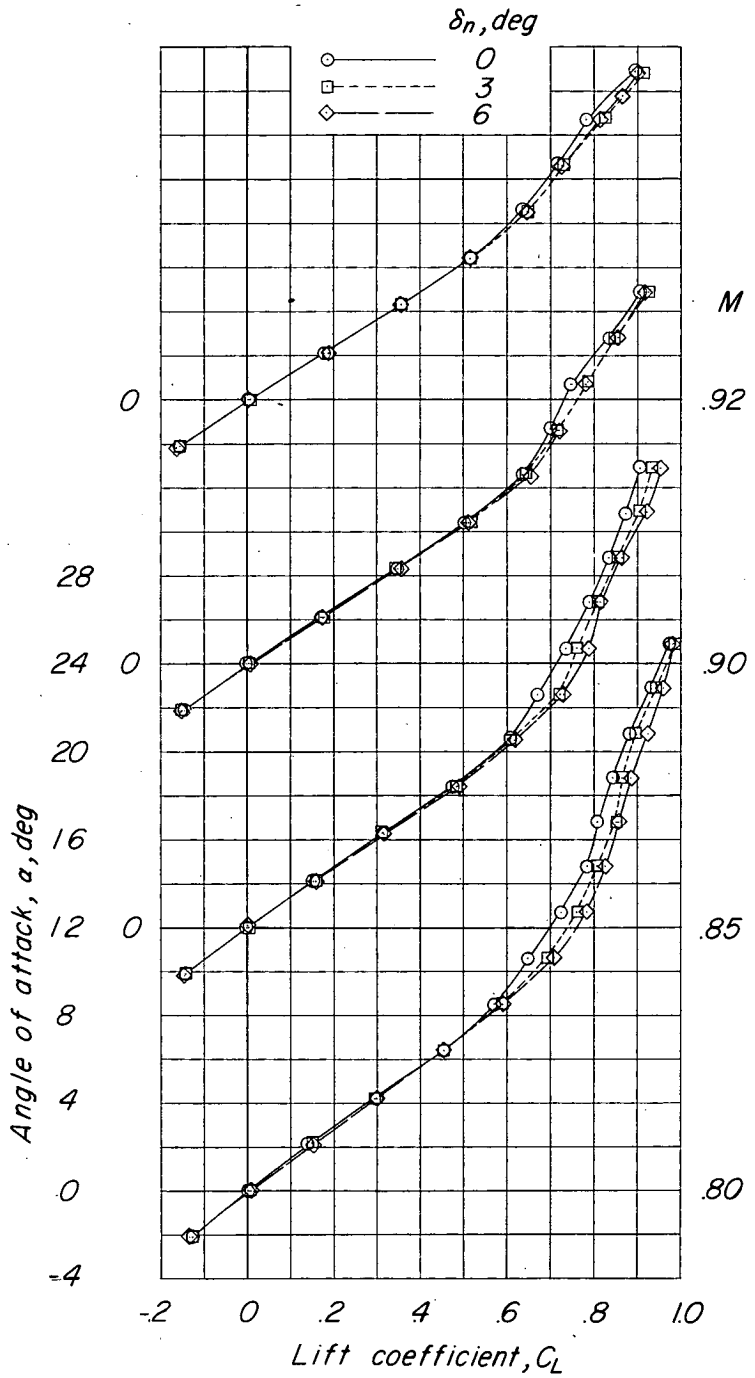

(a) Variation of α with C_L.

Figure 4.- Aerodynamic characteristics of the sharp leading-edge wing-fuselage combination showing effects of full-span leading-edge flaps.

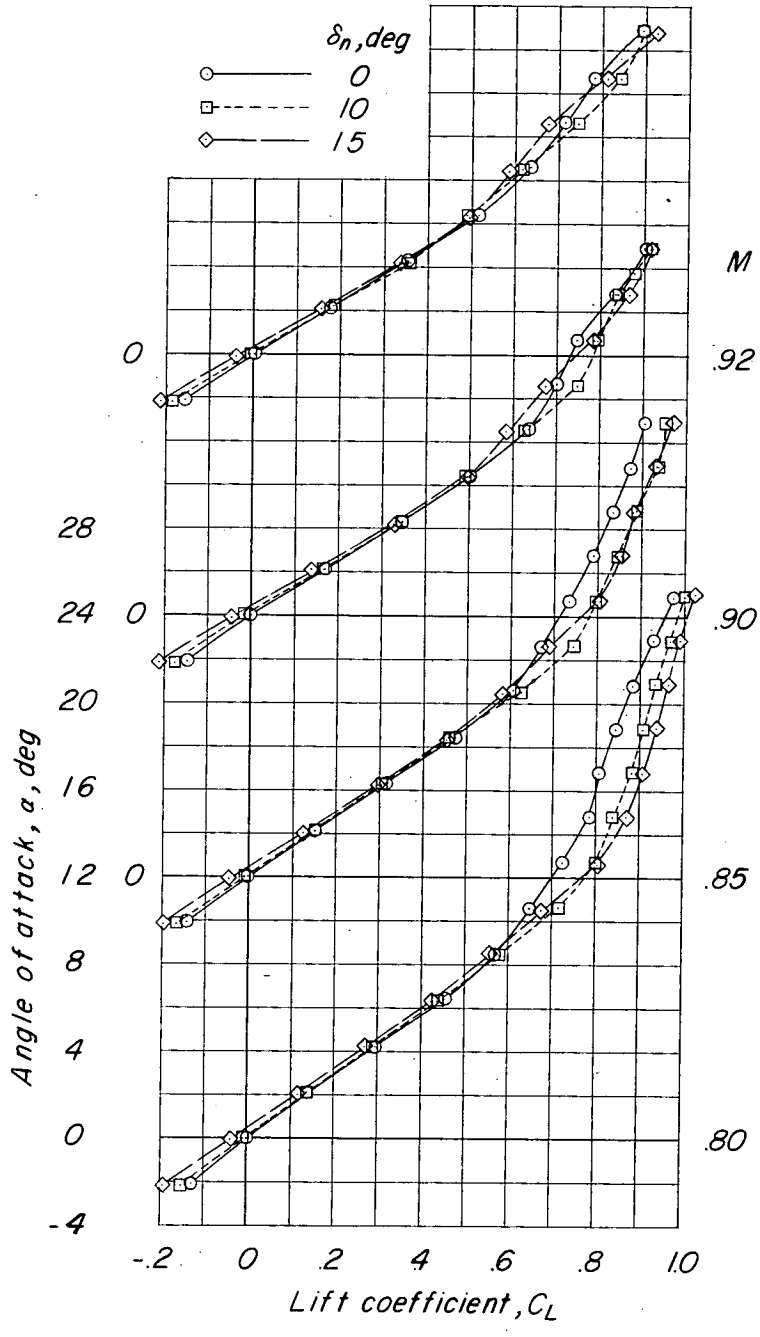

(a) Concluded.

Figure 4.- Continued.

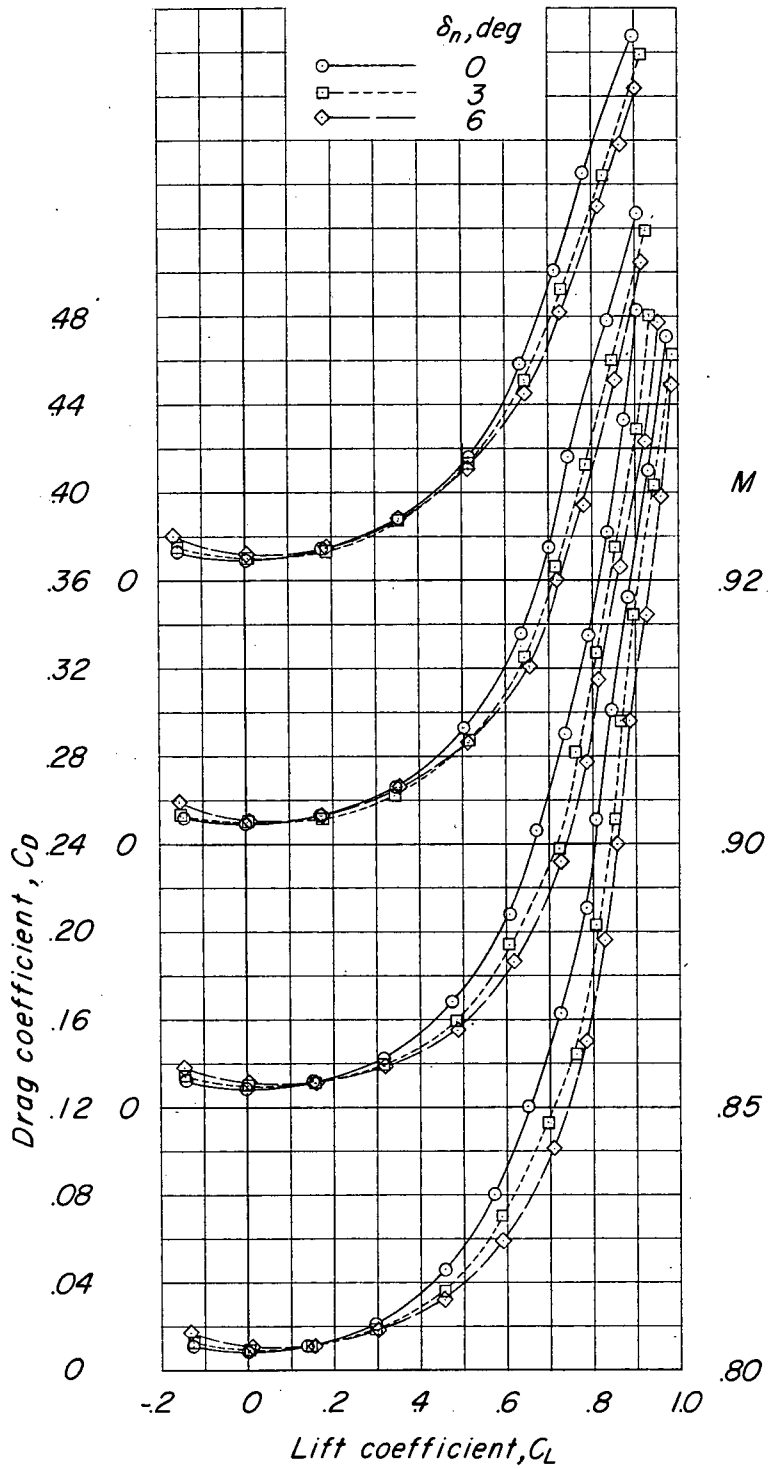

(b) Variation of C_D with C_L.

Figure 4.- Continued.

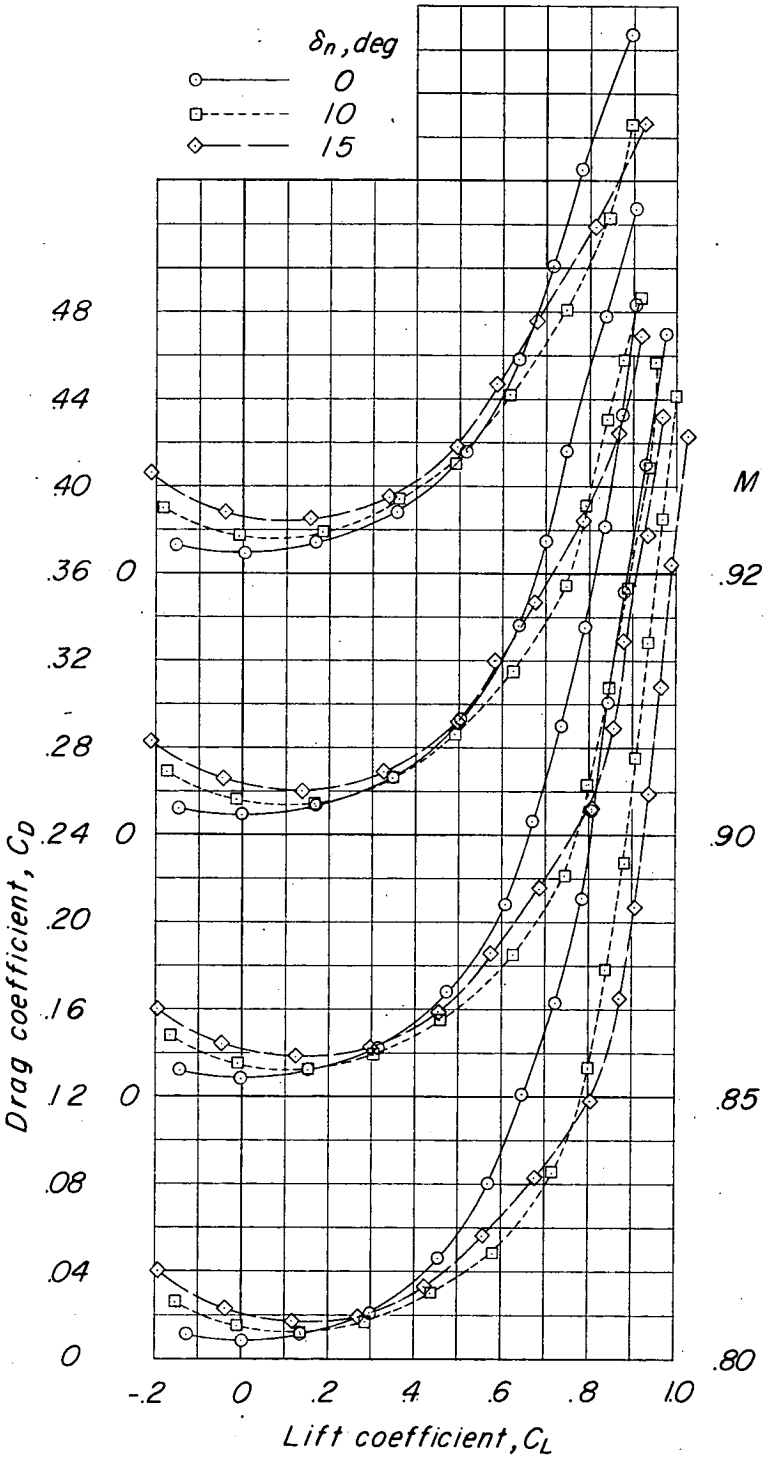

(b) Concluded.

Figure 4.- Continued.

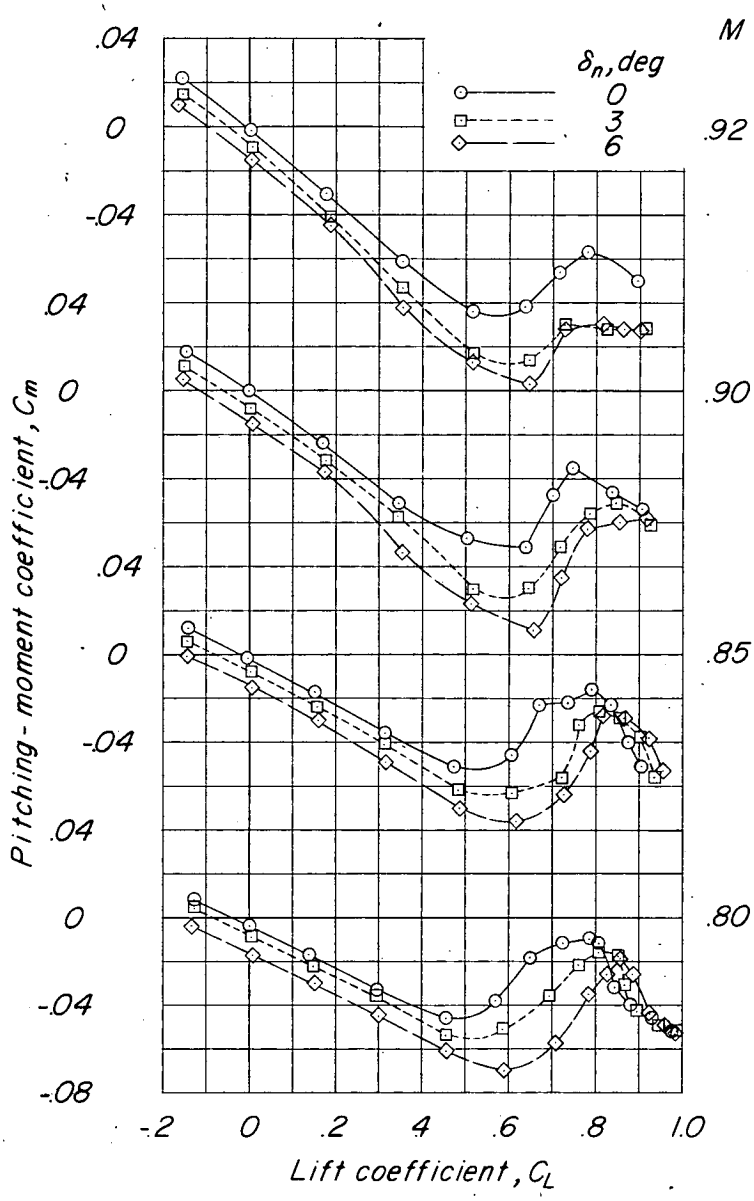

(c) Variation of C_m with C_L.

Figure 4.- Continued.

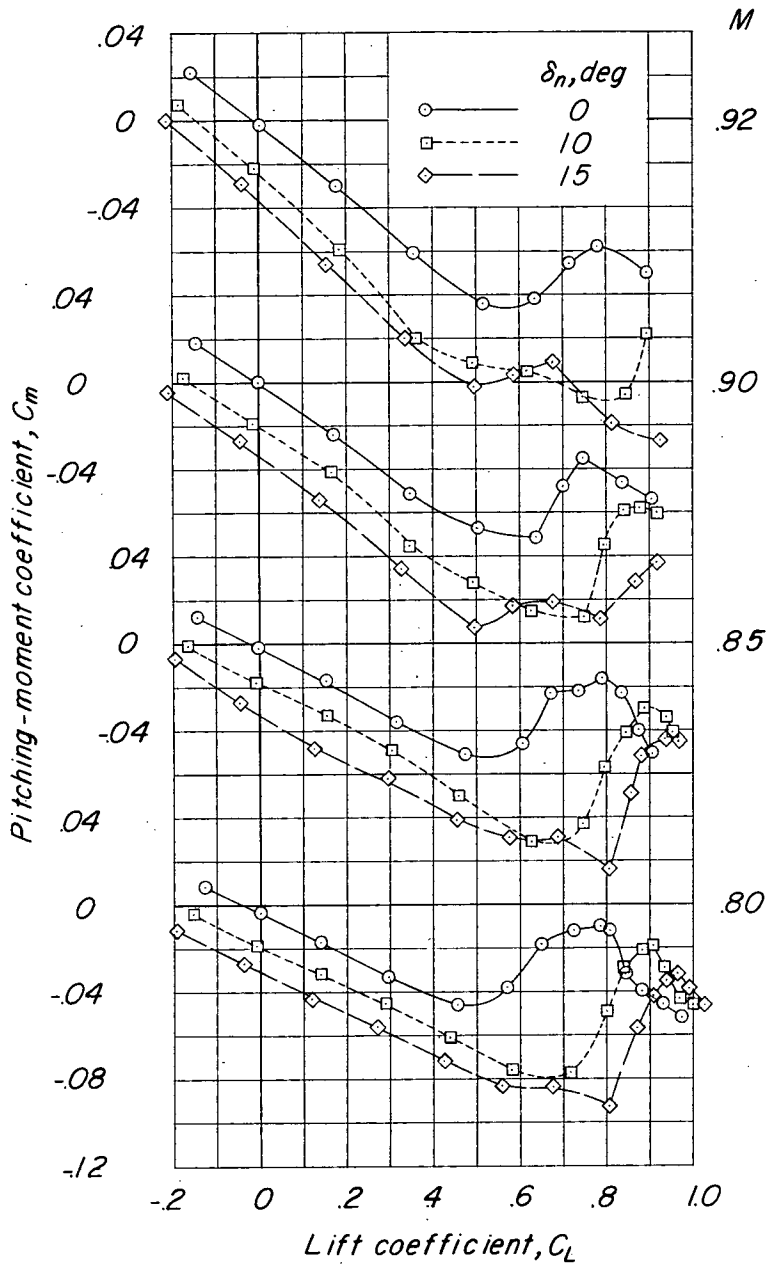

(c) Concluded.

Figure 4.- Continued.

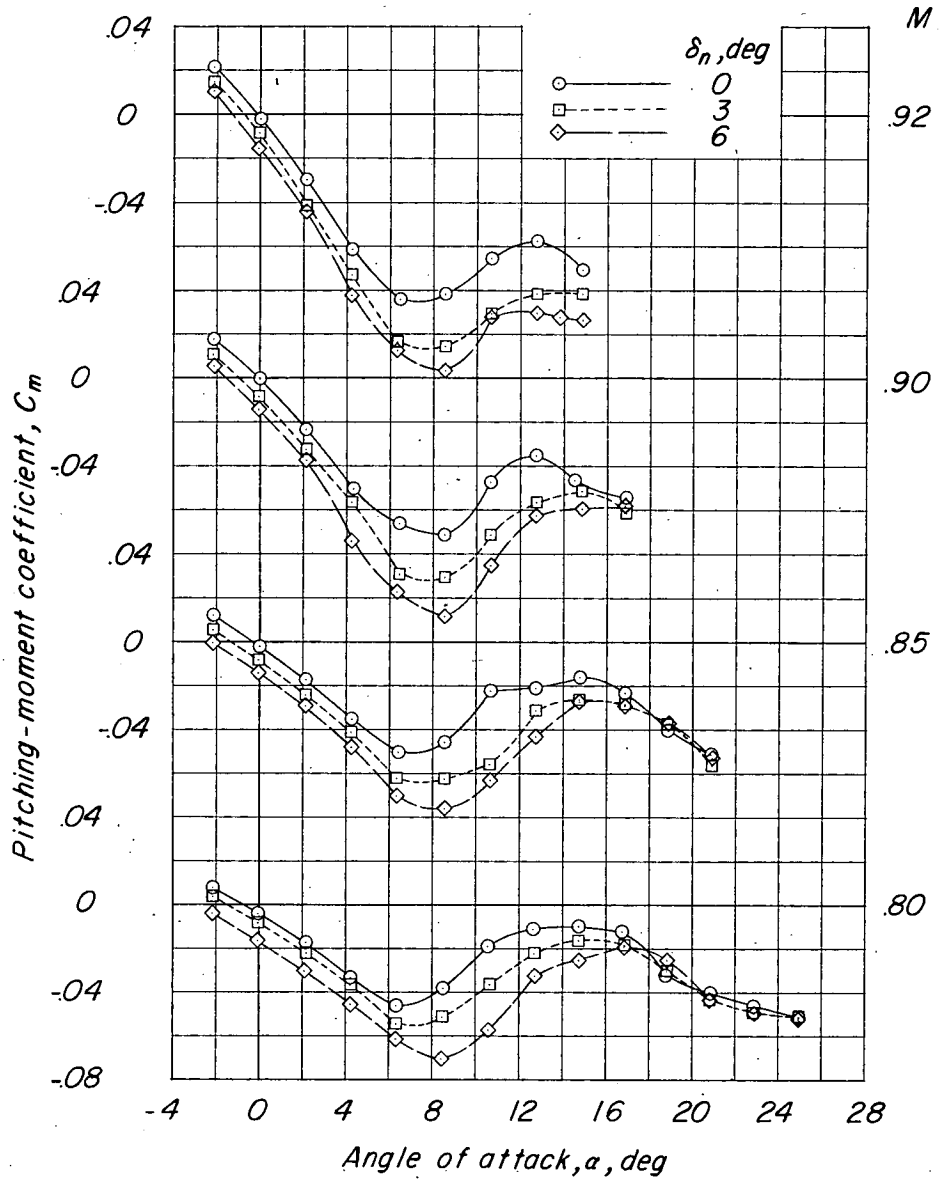

(d) Variation of C_m with α.

Figure 4.- Continued.

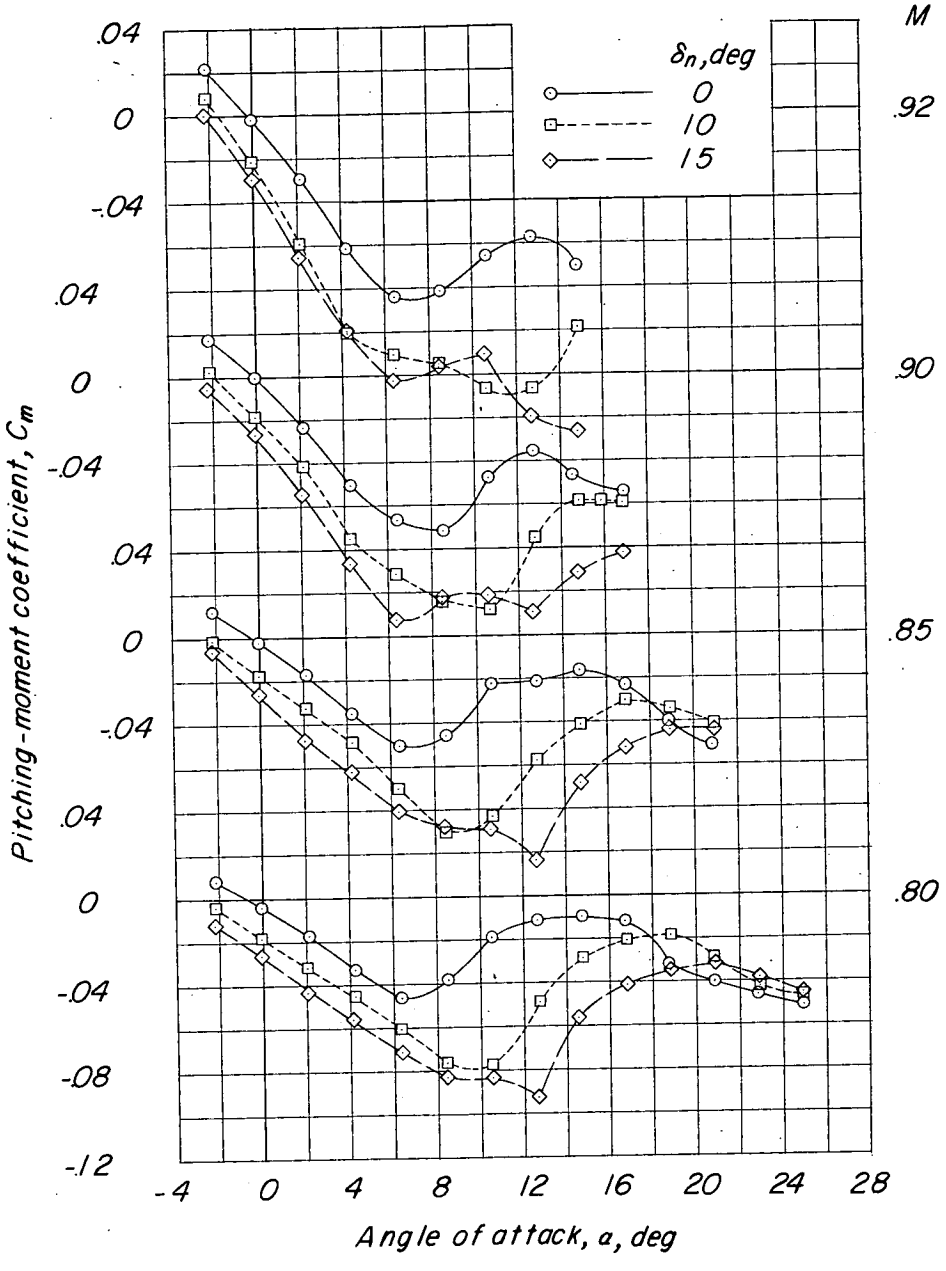

(d) Concluded.

Figure 4.- Concluded.

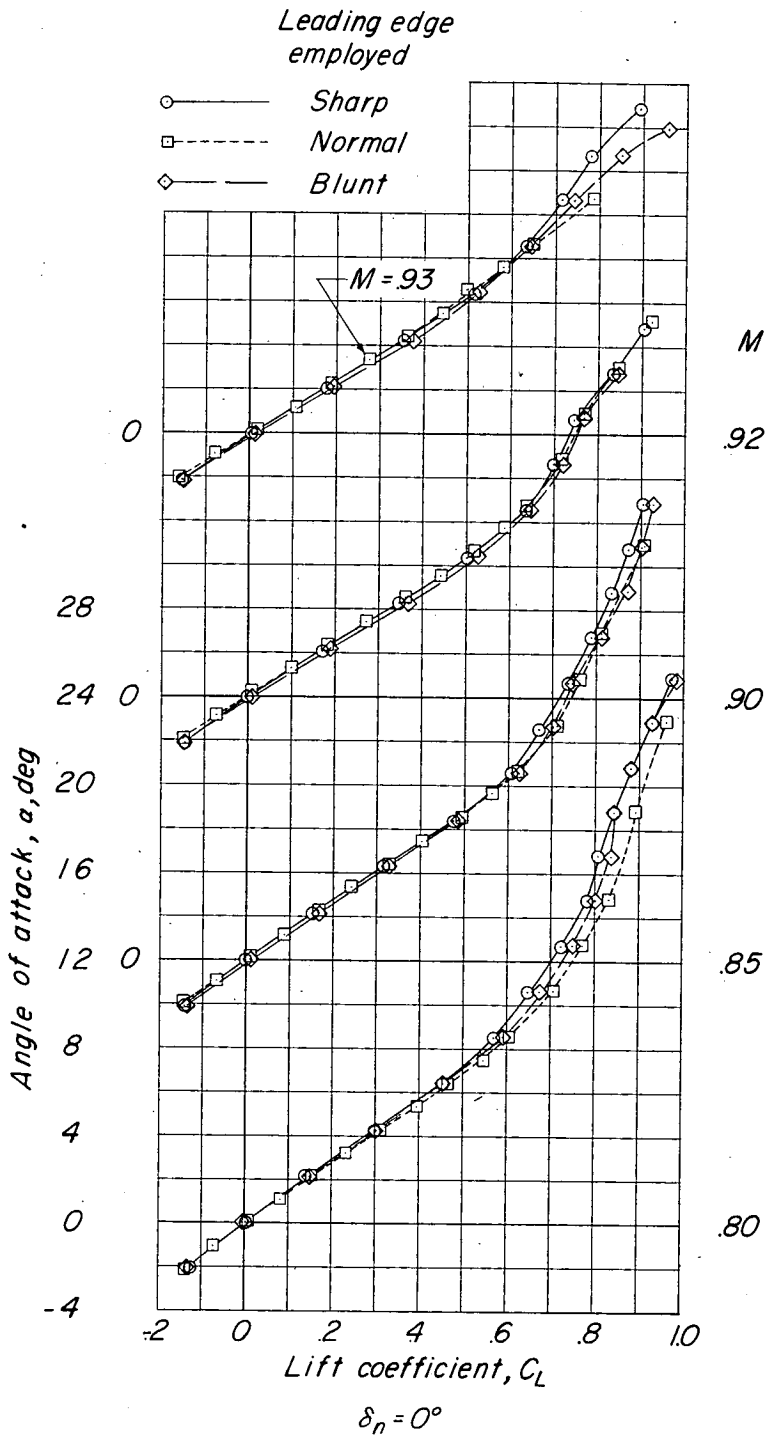

(a) Variation of α with C_L.

Figure 5.- Aerodynamic characteristics of wing-fuselage combination showing effects of leading-edge radius.

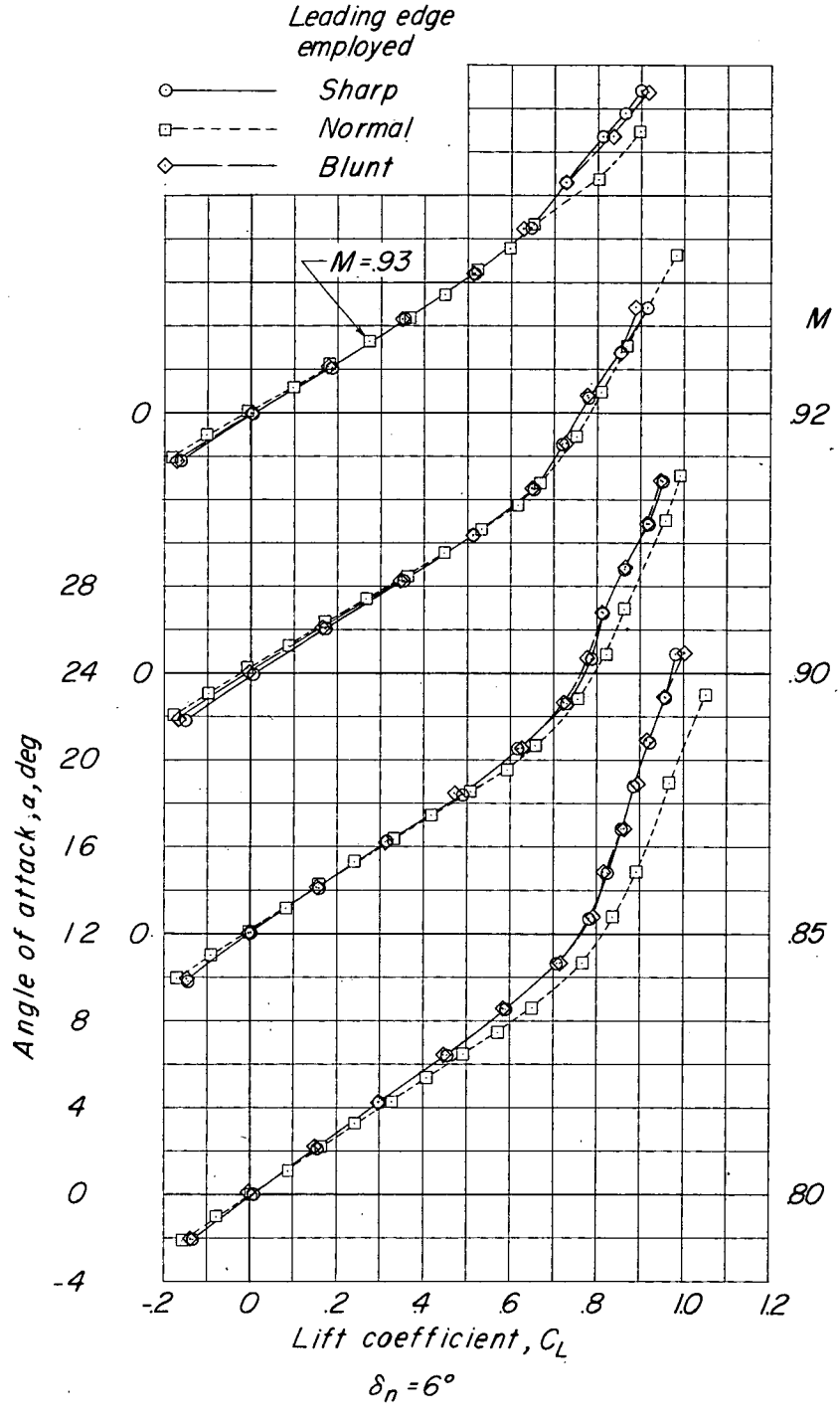

(a) Concluded.

Figure 5.- Continued.

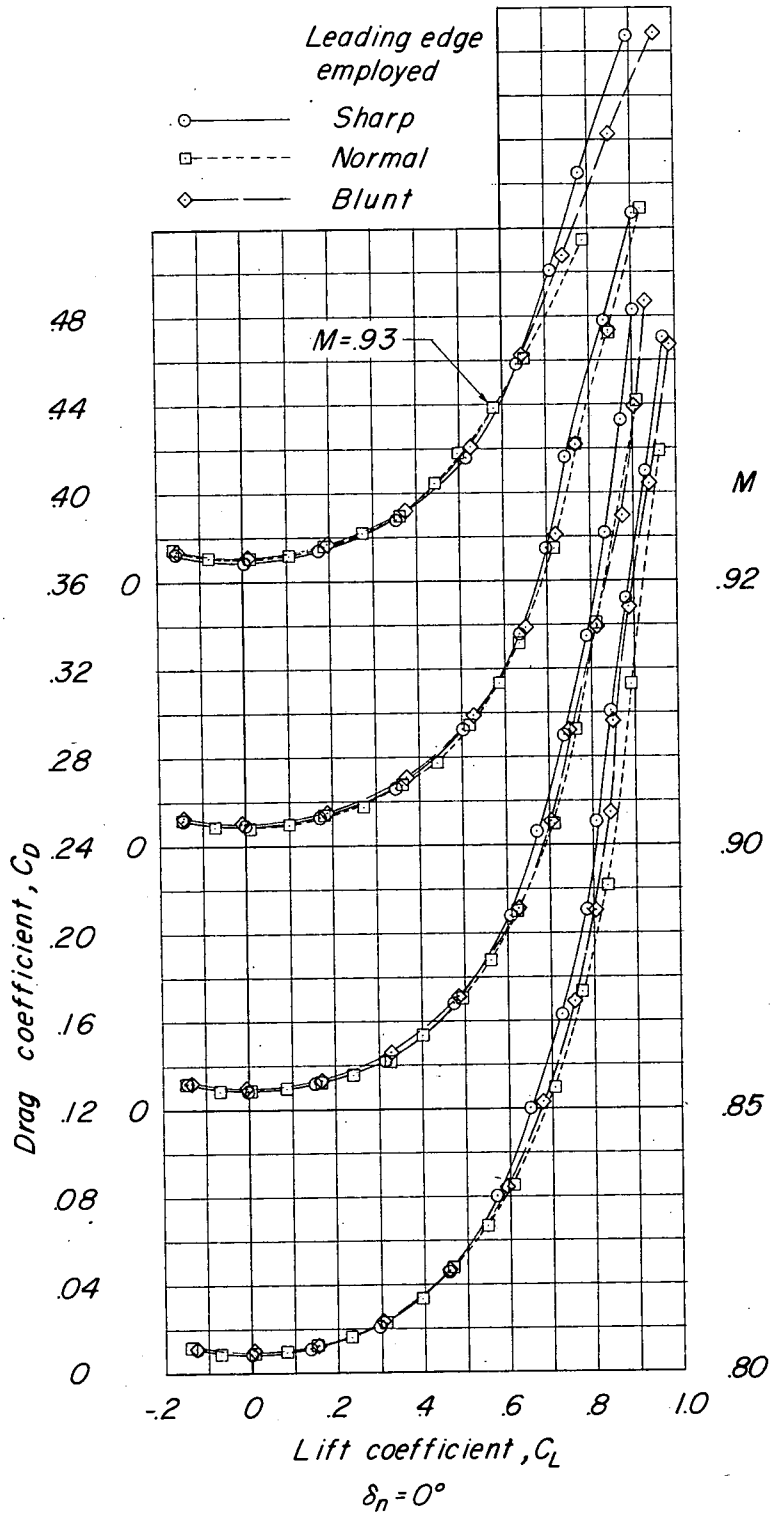

(b) Variation of C_D with C_L.

Figure 5.- Continued.

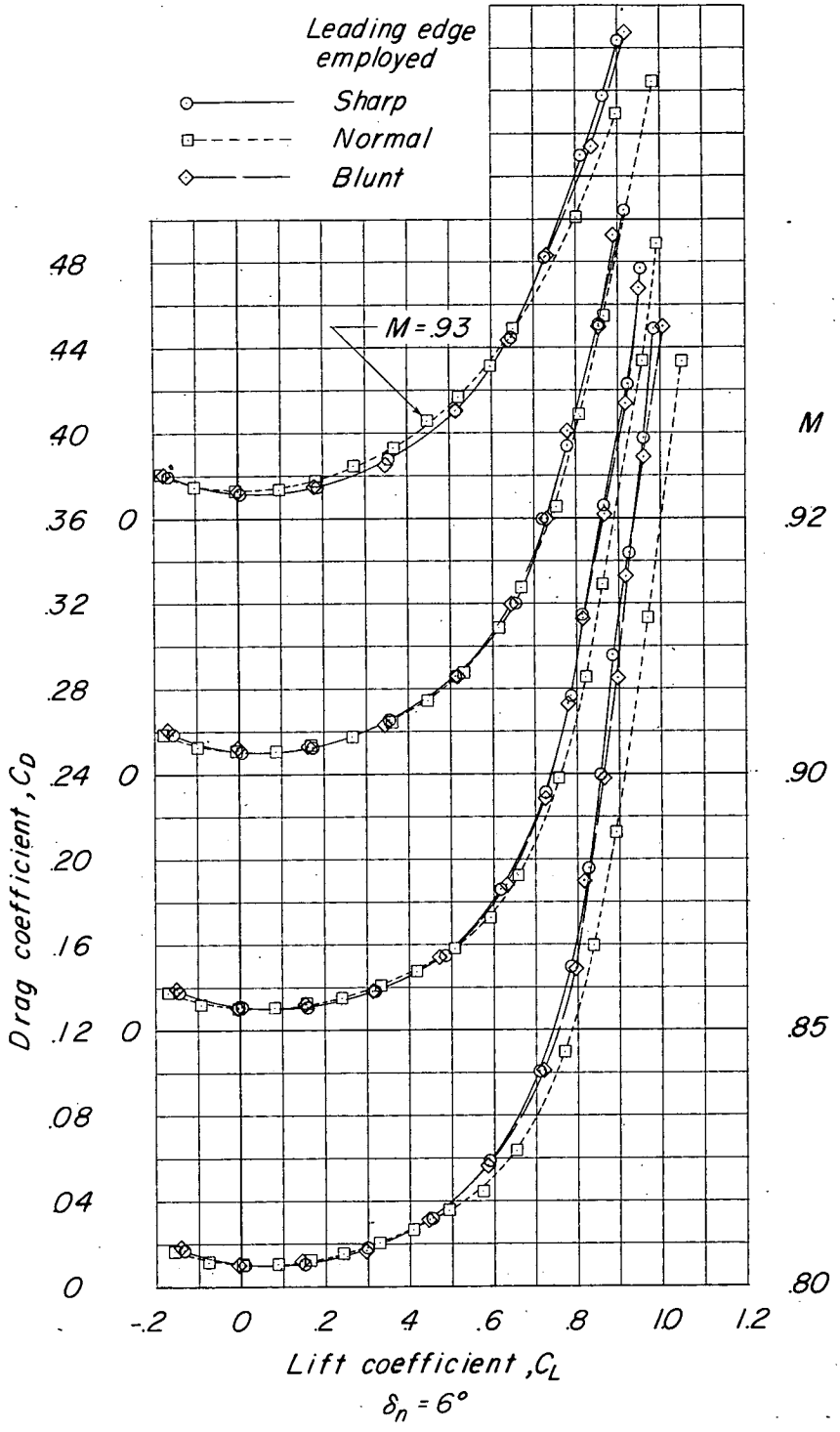

(b) Concluded.

Figure 5.- Continued.

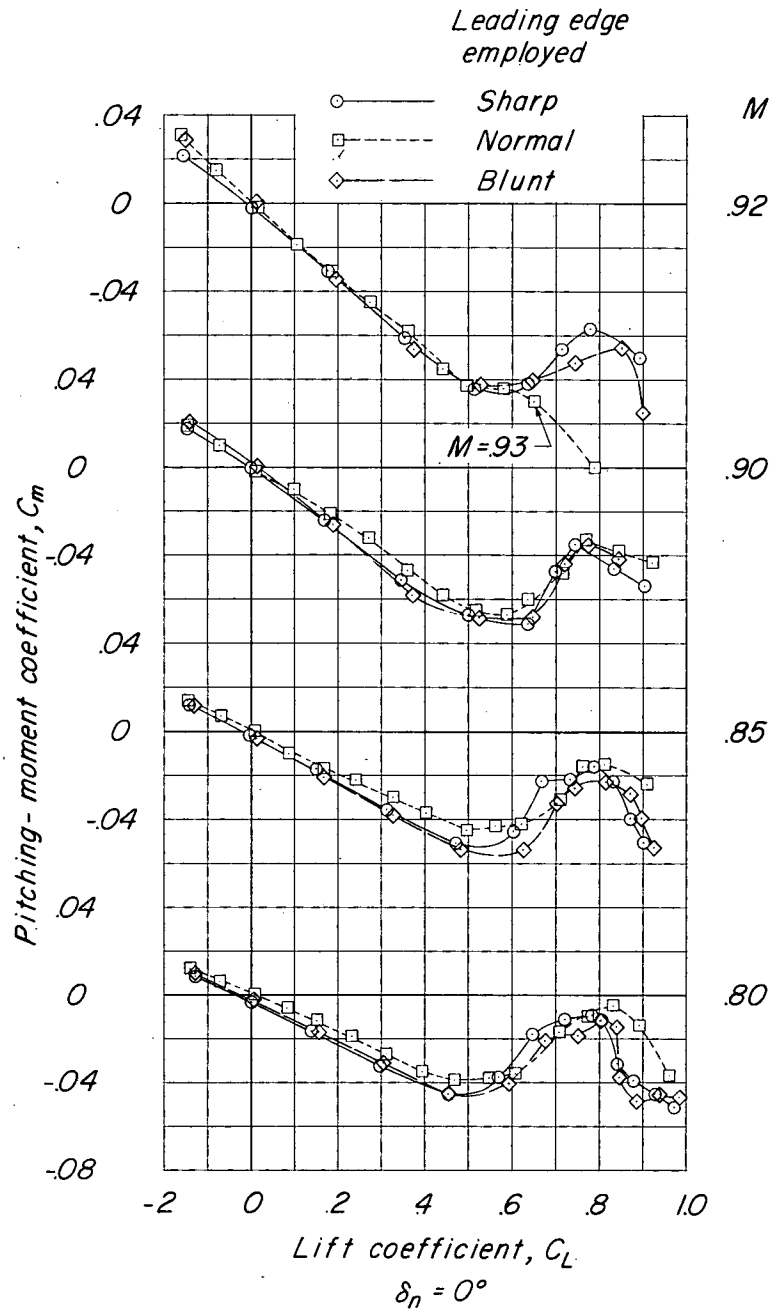

(c) Variation of C_m with C_L.

Figure 5.- Continued.

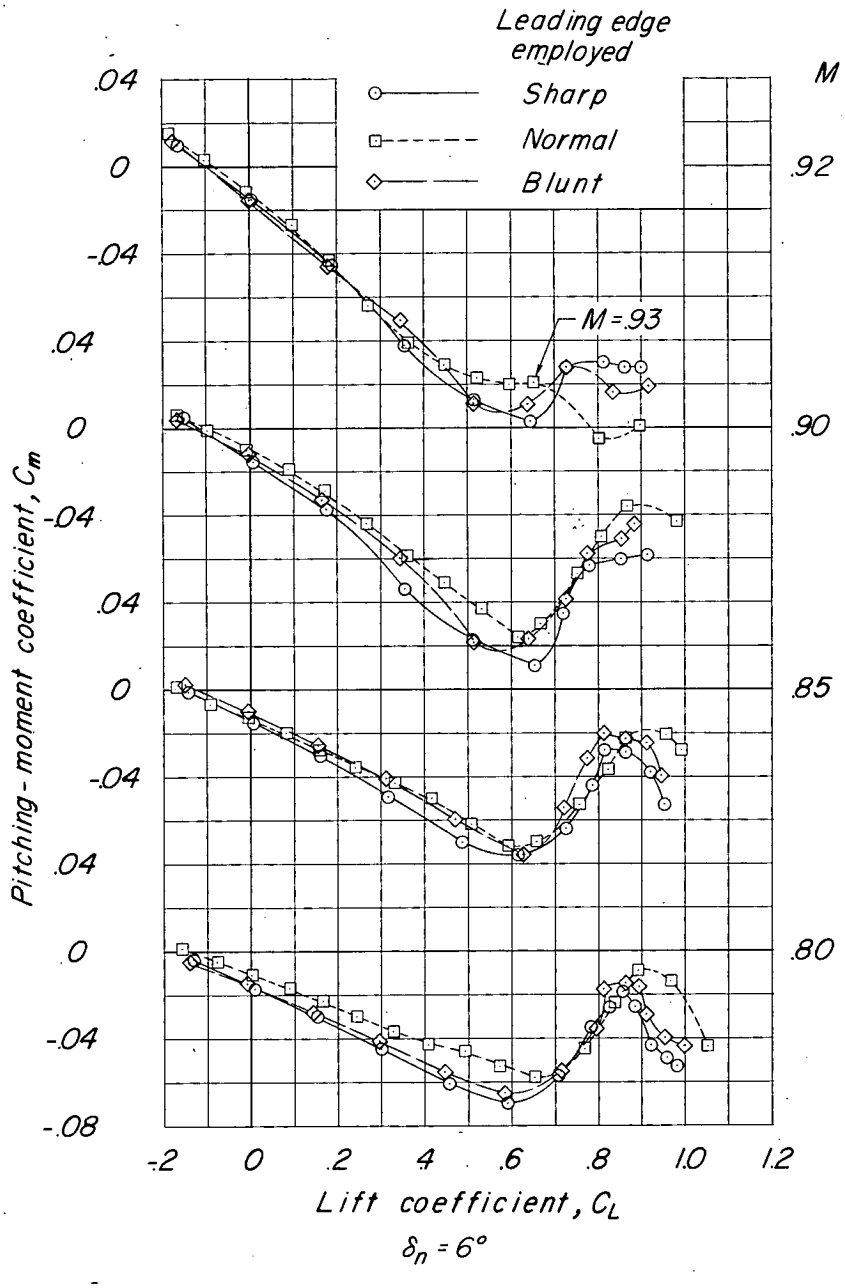

(c) Concluded.

Figure 5.- Continued.

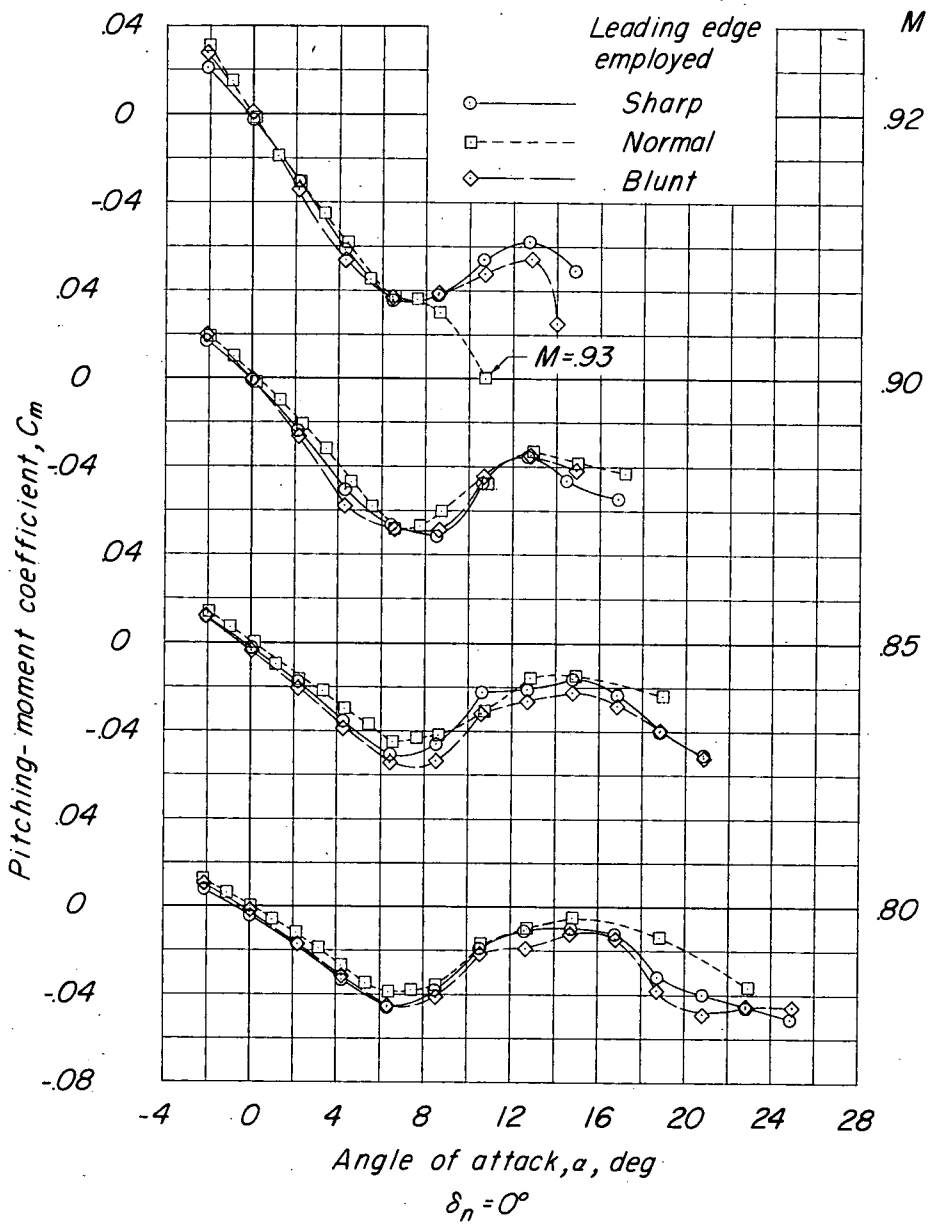

(d) Variation of C_m with α.

Figure 5.- Continued.

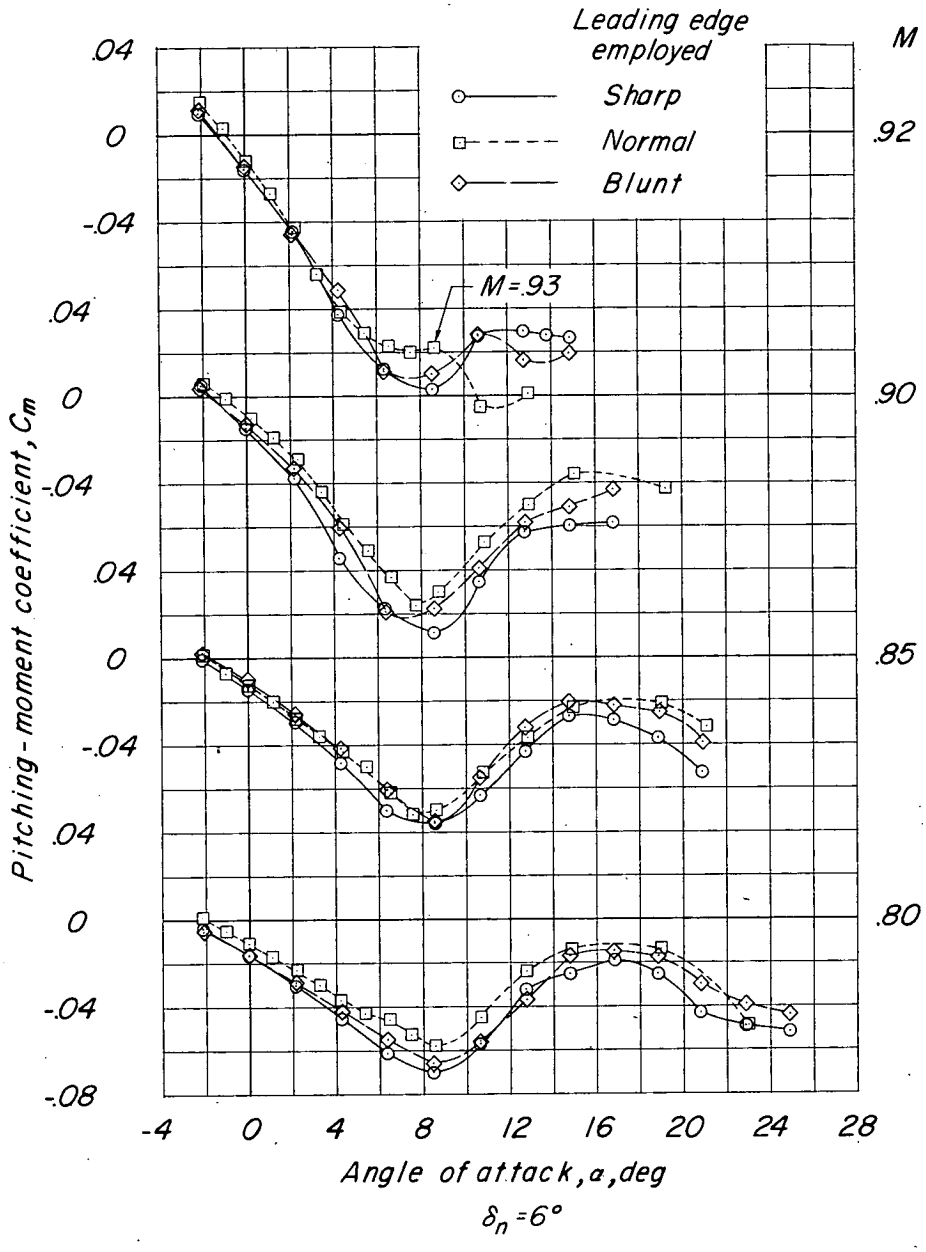

(d) Concluded.

Figure 5.- Concluded.

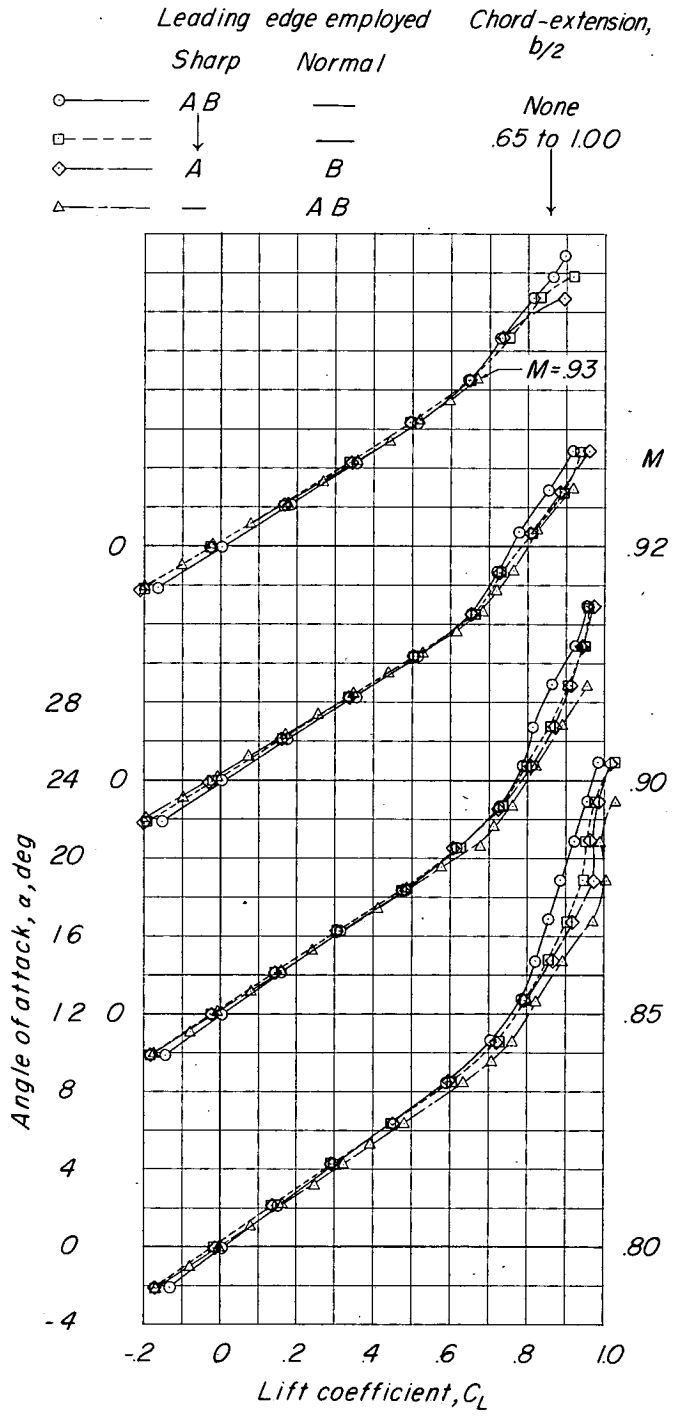

(a) Variation of α with C_L.

Figure 6.- Aerodynamic characteristics of wing-fuselage combination showing effects of leading-edge radius and chord extensions. $\delta_n = 6^\circ$.

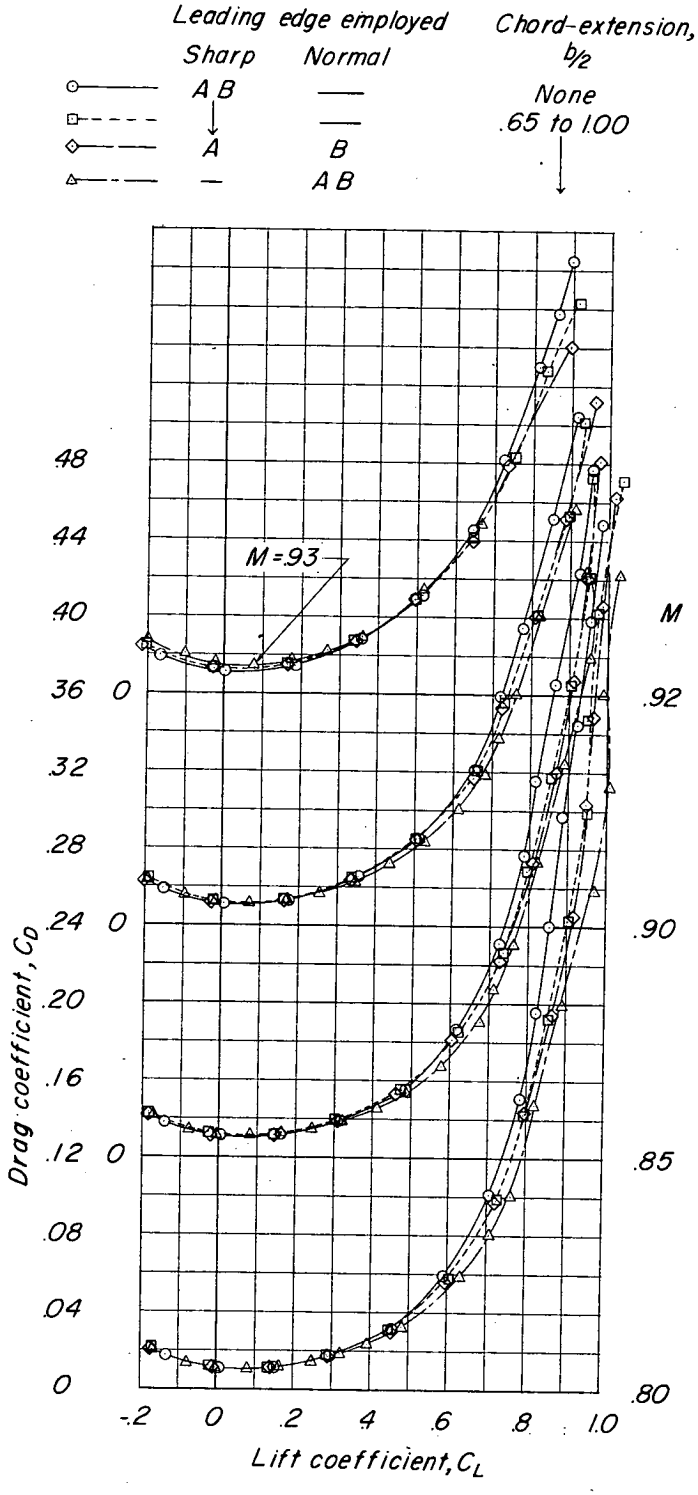

(b) Variation of C_D with C_L.

Figure 6.- Continued.

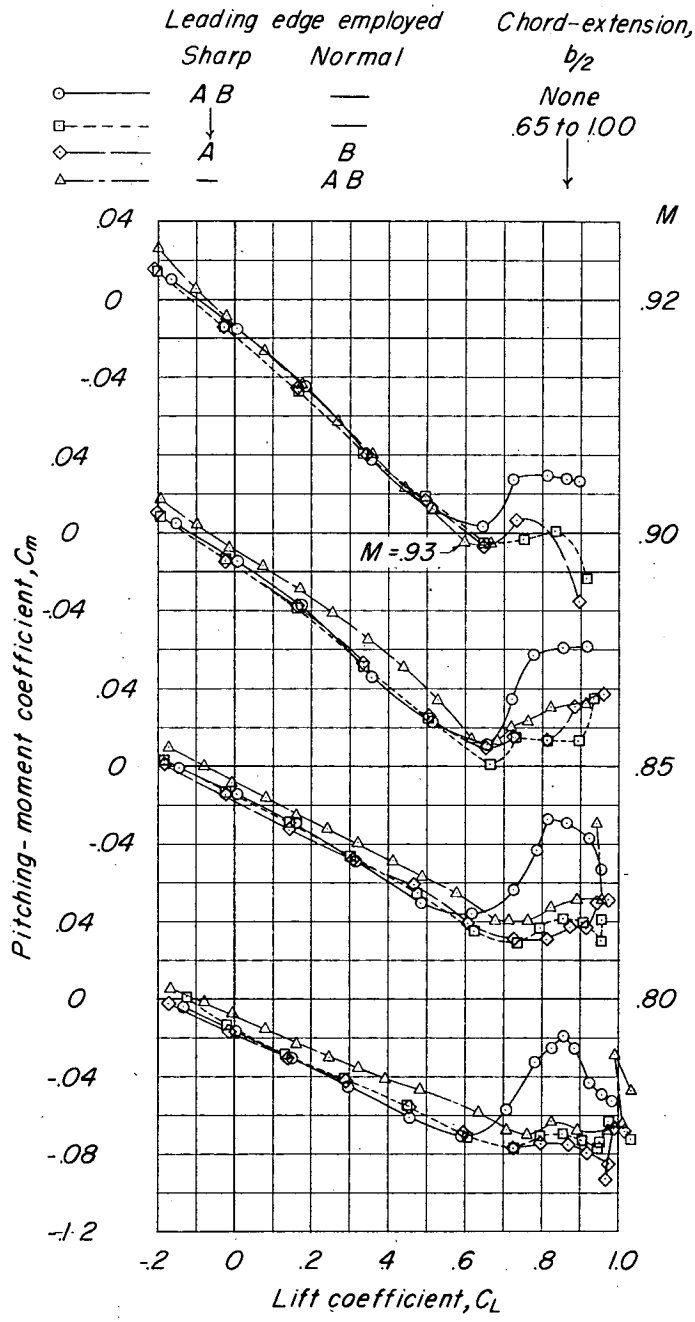

(c) Variation of C_m with C_L.

Figure 6.- Continued.

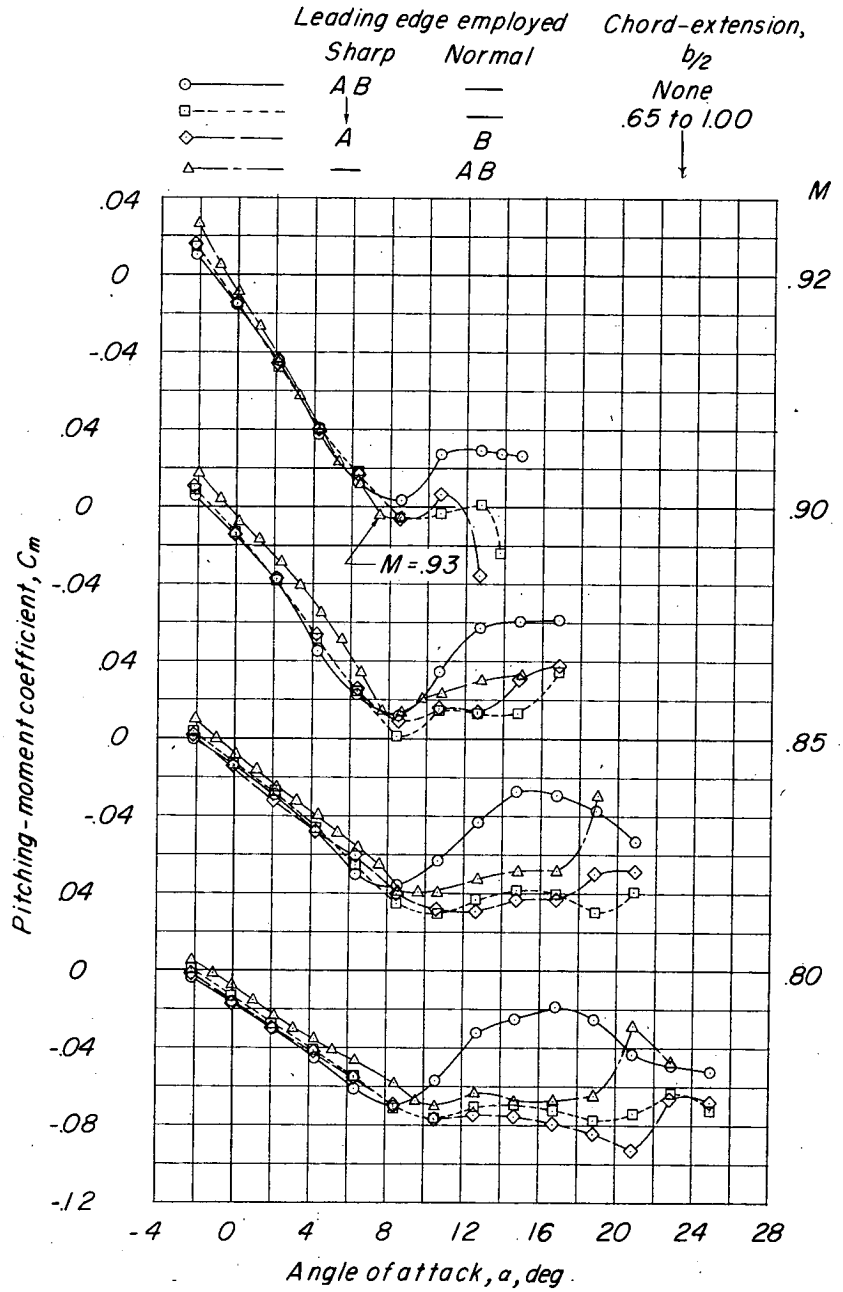

(d) Variation of C_m with α.

Figure 6.- Concluded.

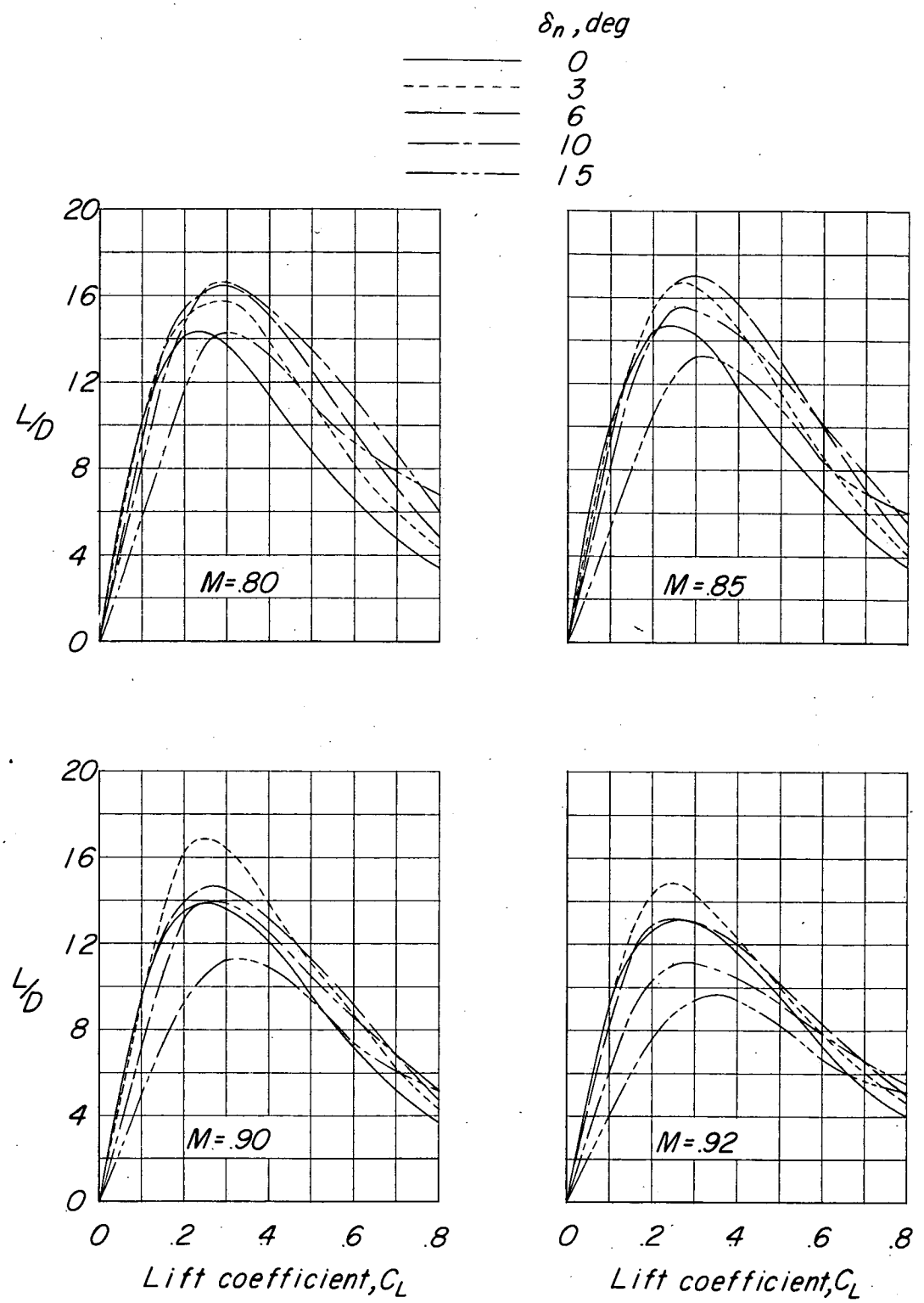

Figure 7.- Lift-drag ratios of sharp leading-edge wing-fuselage combination showing effects of leading-edge flaps.

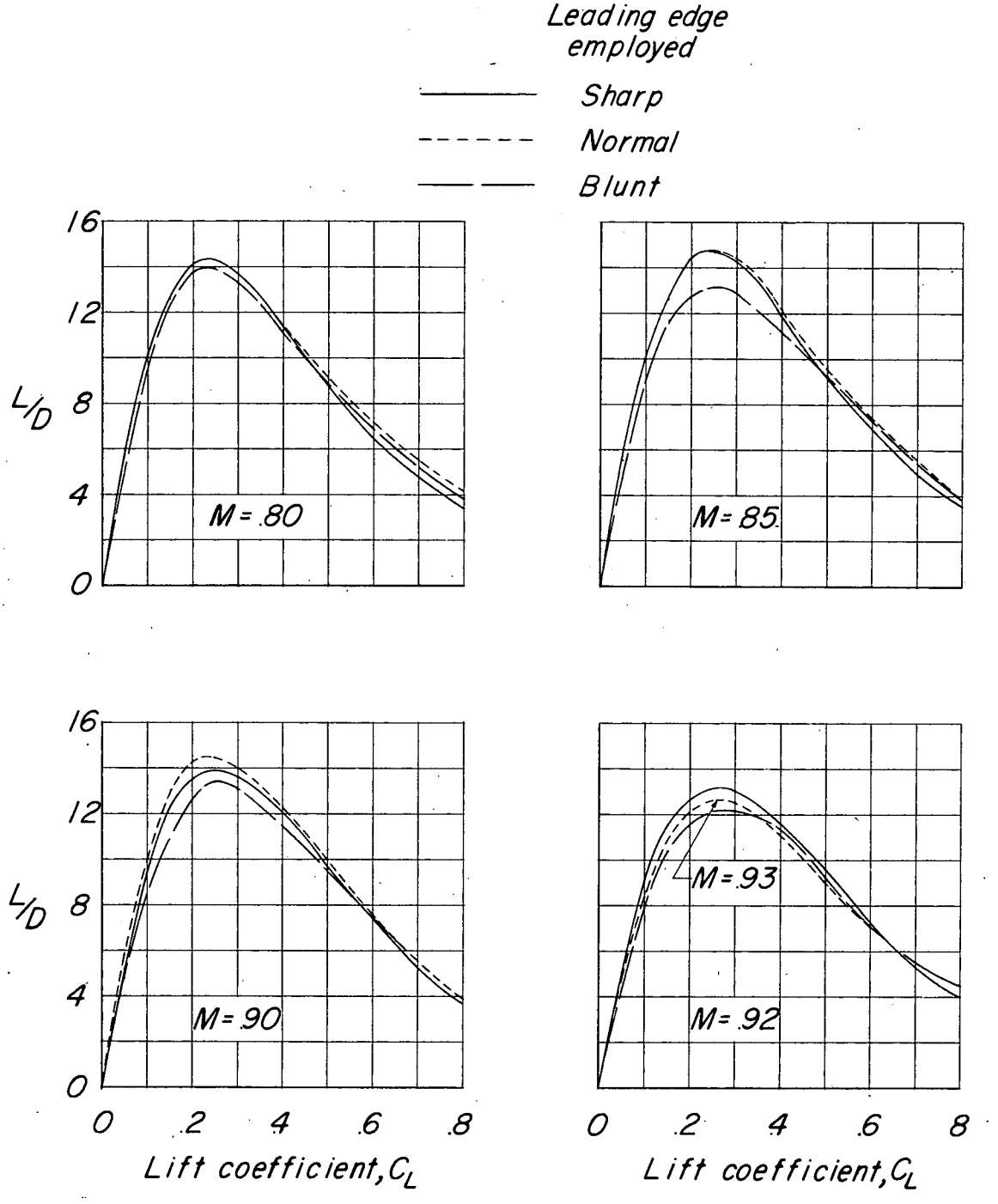

Figure 8.- Lift-drag ratios of wing-fuselage combination showing effects of leading-edge radius. $\delta_n = 0^o$.

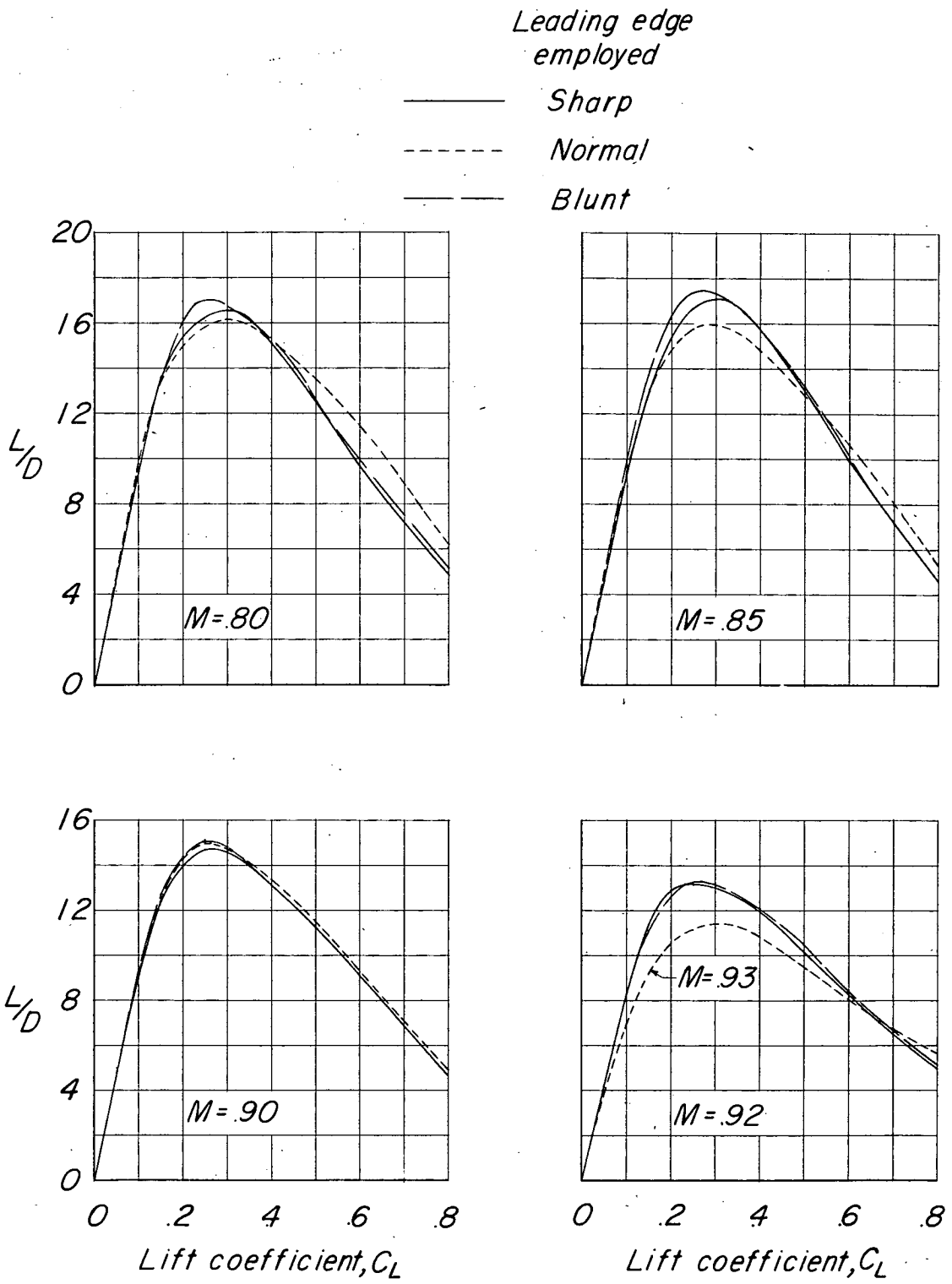

Figure 9.- Lift-drag ratios of wing-fuselage combination showing effects of leading-edge radius. $\delta_n = 6^\circ$.

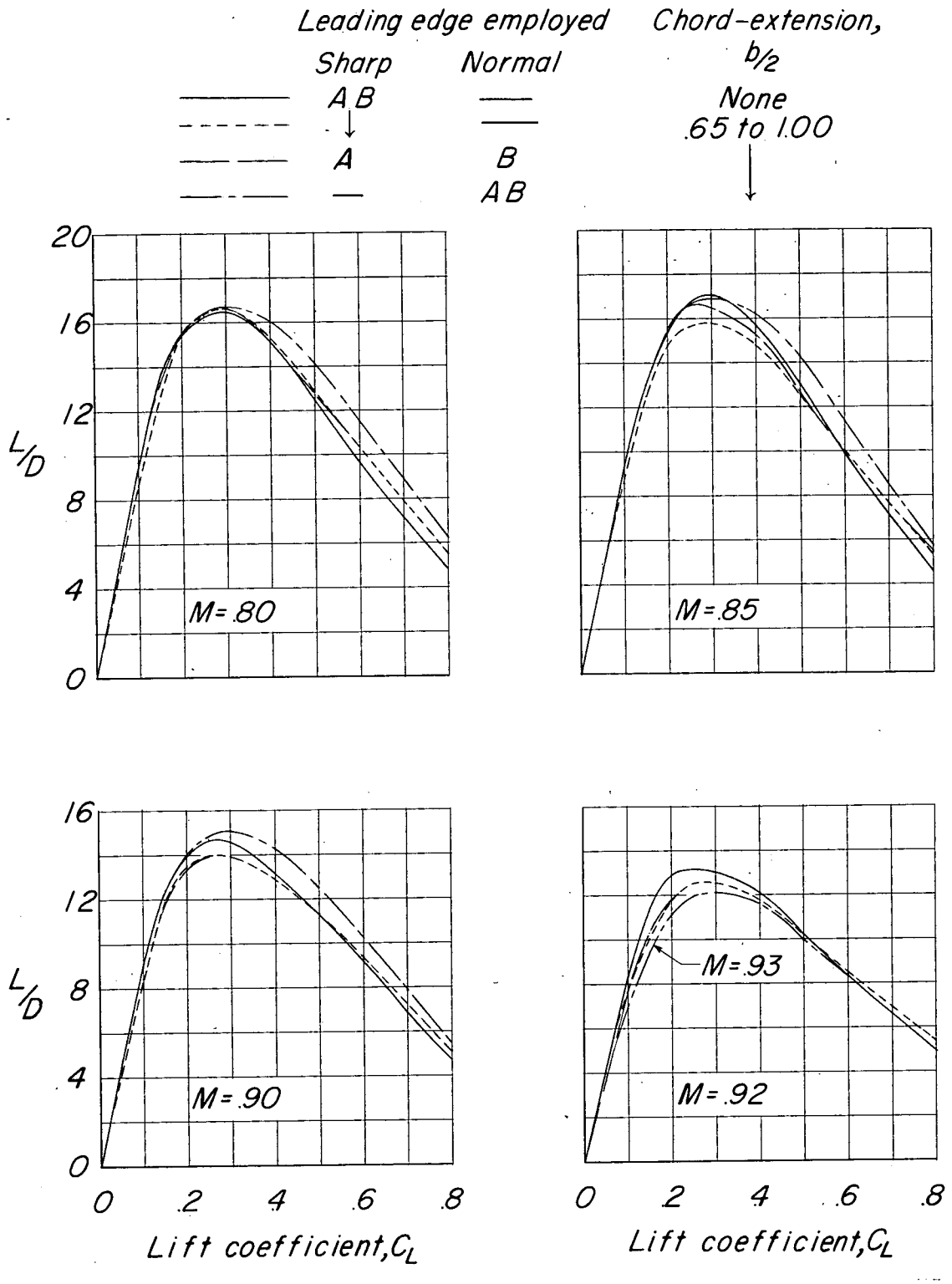

Figure 10.- Lift-drag ratios of wing-fuselage combination showing effects of leading-edge radius and chord-extensions. $\delta_n = 6^o$.

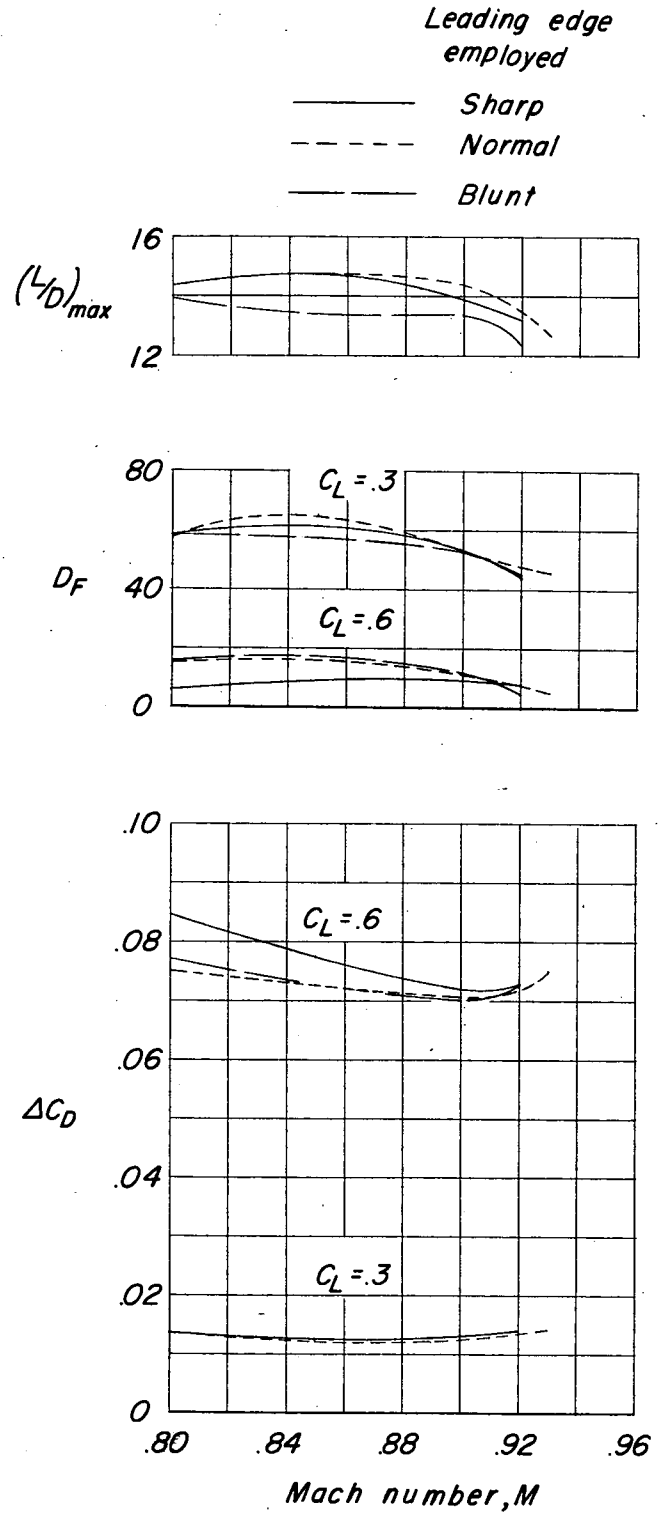

Figure 11.- Summary of drag characteristics showing effect of leading-edge radius. $\delta_n = 0^\circ$.

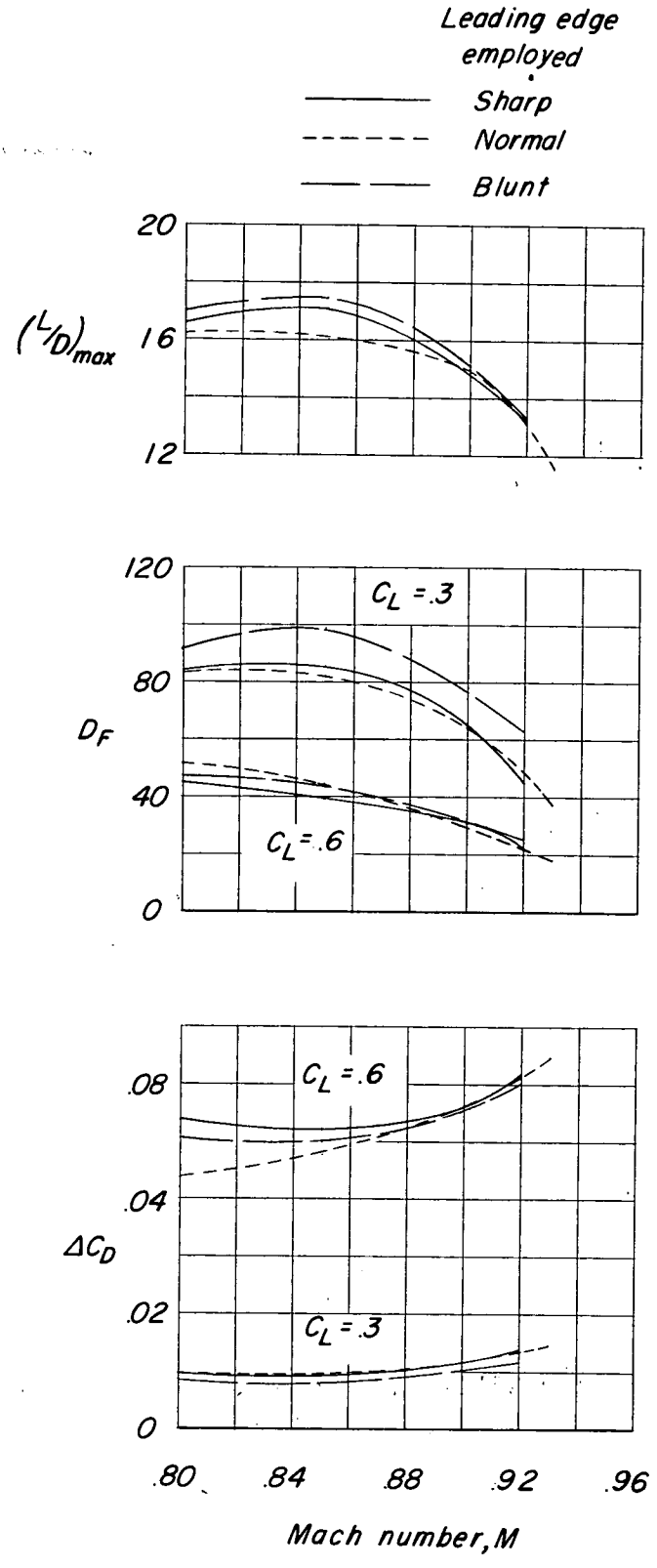

Figure 12.- Summary of drag characteristics showing effect of leading-edge radius. $\delta_n = 6^\circ$.

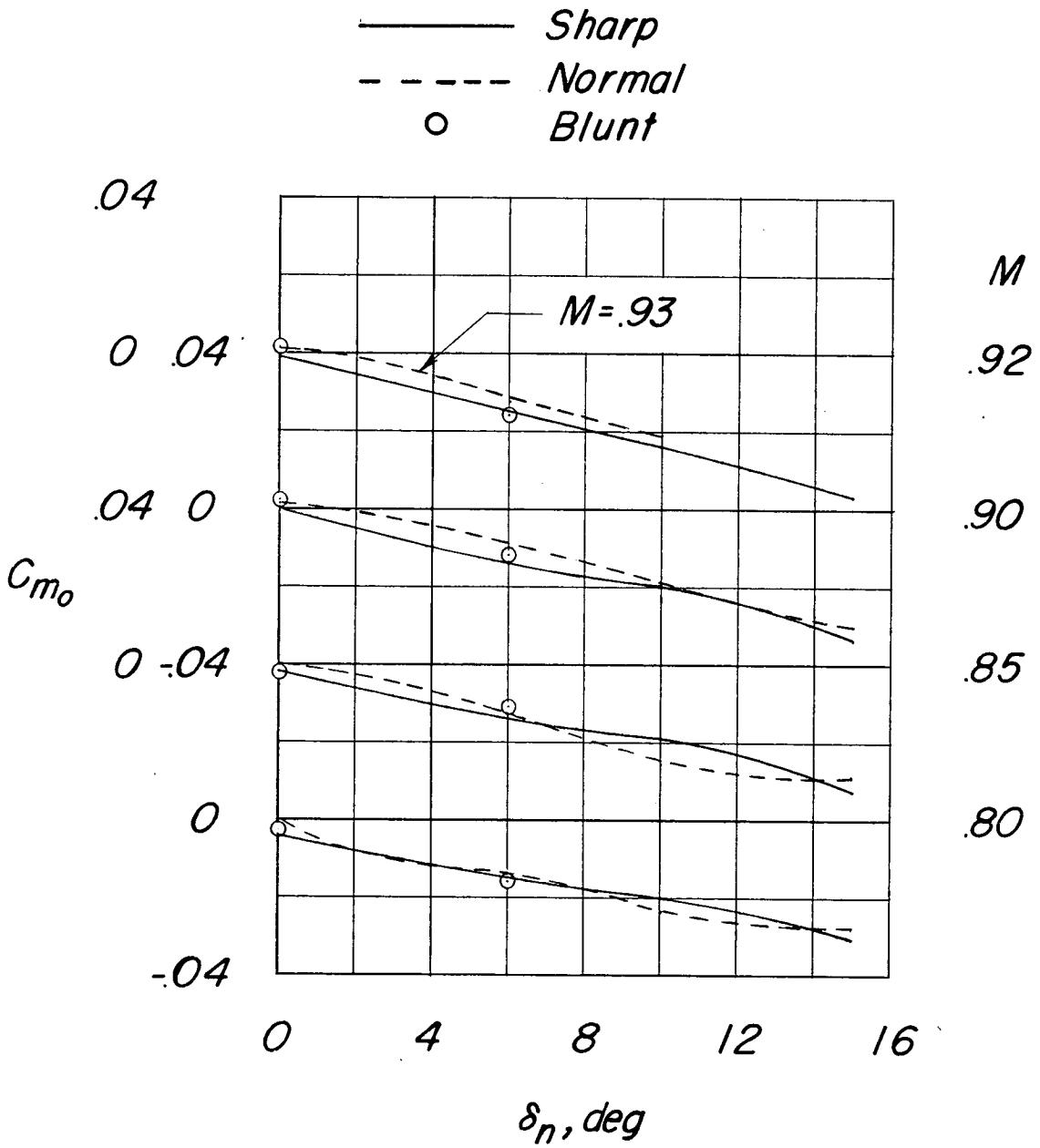

Figure 13.- Effect of leading-edge radius on C_{m_o} through leading-edge flap-deflection range.